JBC Papers in Press. Published on May 10, 2016 as Manuscript M116.728014
The latest version is at http://www.jbc.org/cgi/doi/10.1074/jbc.M116.728014

Direct Comparison of Manganese Detoxification/Efflux Proteins and Molecular Characterization of ZnT10 as a Manganese Transporter

Yukina Nishito[1], Natsuko Tsuji[1], Hitomi Fujishiro[2], Taka-aki Takeda[1], Tomohiro Yamazaki[1†], Fumie Teranishi[1], Fumiko Okazaki[3#], Ayu Matsunaga[3], Karin Tuschl[4], Rajini Rao[5], Satoshi Kono[6], Hiroaki Miyajima[6], Hiroshi Narita[3], Seiichiro Himeno[2], and Taiho Kambe[1]

From the [1]Division of Integrated Life Science, Graduate School of Biostudies, Kyoto University, Kyoto 606-8502, Japan; the [2]Faculty of Pharmaceutical Sciences, Tokushima Bunri University, Tokushima 770-8514, Japan; the [3]Department of Food Science, Kyoto Women's University, Kyoto 605-8501, Japan; the [4]Clinical and Molecular Genetics Unit, University College London Institute of Child Health, London WC1N 1EH, UK; the [5]Department of Physiology, School of Medicine, The Johns Hopkins University, Baltimore, MD 21205, USA; and the [6]First Department of Medicine, Hamamatsu University School of Medicine, Hamamatsu 431-3192, Japan

[†]Present address: Institute for Genetic Medicine, Hokkaido University, Sapporo 060-0815, Japan

[#]Present address: Faculty of Agriculture, Ryukoku University, Ohtsu, Shiga 520-2194, Japan

Running title: *Molecular characterization of ZnT10 as a Mn transporter*

To whom correspondence should be addressed: Taiho Kambe, Division of Integrated Life Science, Graduate School of Biostudies, Kyoto University, Kyoto 606-8502, Japan. Tel.: +81-75-753-6273; Fax: +81-75-753-6274; E-mail: kambe1@kais.kyoto-u.ac.jp

Keywords: zinc, manganese, transporter, metal homeostasis, substrate specificity, efflux, SPCA1, ferroportin, ATP13A family protein

ABSTRACT

Manganese (Mn) homeostasis involves coordinated regulation of specific proteins involved in Mn influx and efflux. However, the proteins that are involved in detoxification/efflux have not been completely resolved, nor has the basis by which they select their metal substrate. Here, we compared six proteins, which were reported to be involved in Mn detoxification/efflux, by evaluating their ability to reduce Mn toxicity in chicken DT40 cells, finding that human ZnT10 (hZnT10) was the most significant contributor. A domain swapping and substitution analysis between hZnT10 and a zinc-specific transporter hZnT1 showed that residue N43, which corresponds to the His residue constituting the potential intramembranous zinc coordination site in other ZnT transporters, is necessary to impart hZnT10's unique Mn mobilization activity; residues C52 and L242 in transmembrane domains II and V play a subtler role in controlling the metal specificity of hZnT10. Interestingly, the H->N reversion mutant in hZnT1 conferred Mn transport activity and loss of zinc transport activity. These results provide important information about Mn detoxification/efflux mechanisms in vertebrate cells as well as the molecular characterization of hZnT10 as a Mn transporter.

Manganese (Mn) is an essential trace element. Mn is a key cofactor for a variety of enzymes, including glutamine synthetase, superoxide dismutase 2, decarboxylases, and sugar transferases, and thus is indispensable for central nervous system functions, immune functions, and carbohydrate metabolism (1,2). At elevated levels, however, Mn is toxic and exposure to this trace element has been associated with various pathogeneses,

including a neurological syndrome called manganism, whose symptoms resemble those of Parkinson disease (3,4). For these reasons, Mn homeostasis must be tightly controlled at a systemic and cellular level. Much of our current understanding of Mn homeostatic mechanisms is derived from genetic studies of *Saccharomyces cerevisiae* (reviewed in (5,6)), which reveals that a number of membrane transporter/channel proteins contribute to the control of Mn homeostasis. Based on these results, the Mn import system, *i.e.*, Mn transport in the direction of the cytosol, has been extensively investigated in vertebrate cells (7-9). Two ZIP zinc (Zn) transporters ZIP8 and ZIP14, known to function as Zn uptake proteins, are involved in Mn uptake from the extracellular site (10,11). In addition, two Nramp transporters Nramp1 and Nramp2/DMT1 are involved in Mn mobilization into the cytosol. Nramp1 acts to mobilize Mn into the cytosol from phagosomes in macrophages, thereby limiting Mn availability to invading microbes (12), whereas Nramp2/DMT1, a major iron transporter, probably functions in the uptake of Mn into the cytosol of all tissue (7). Mn can be transported via other membrane proteins including some types of calcium channels (7,13), although their contribution to cellular Mn homeostasis remains largely unknown.

In contrast, less is known about Mn transporters/channel proteins that participate in Mn detoxification/efflux (13), and further effort is currently needed to completely understand this important process. This is particularly urgent because these transporters/channel proteins may play a role in an established clinical condition caused by excessive Mn accumulation (3,8,14). Of the proteins postulated to be involved in Mn detoxification/efflux, the Golgi-localized secretory pathway Ca^{2+}-ATPase 1 (SPCA1), which is an ortholog of *S. cerevisiae* Pmr1p, is comparatively well characterized (15-17). Moreover, ATP13A2/PARK9 (hereafter ATP13A2) is involved in Mn detoxification (18) based on the observation that the *S. cerevisiae* ortholog Ypk9p protects cells from toxicity of Mn and other metals by vacuolar sequestration (19,20). Importantly, loss-of-function mutations of the *ATP13A2* gene were identified to cause an autosomal recessive form of early-onset parkinsonism (Kufor–Rakeb syndrome; KRS) (21). Recent significant findings show that loss-of-function mutations of the *ZnT10/SLC30A10* gene result in parkinsonism with hypermanganesemia, syndrome of hepatic cirrhosis, polycythemia, and dystonia (22,23). ZnT10 is localized to the plasma membrane and functional in Mn metabolism by effluxing cytosolic Mn (24,25). ZnT10 is also involved in Zn homeostasis in subcellular localization (26,27). The finding that loss-of-function mutations of *ATP13A2* and *ZnT10* genes result in the development of parkinsonism accelerates the necessity to clarify Mn detoxification/efflux mechanisms in cells.

We have previously established chicken DT40 cells as an important model system for studying zinc transporter functions using gene-targeting/re-expression strategies (28–30). This system is useful to explore metal homeostasis and membrane transport protein functions in vertebrate cells because DT40 cells have a similar homeostatic regulation system of metals to that of mammalian cells and allow efficient gene disruption owing to their high homologous recombination activity (31). In this study, we investigated transporter/channel proteins that function in detoxification/efflux of Mn using DT40 cells deficient in the *SPCA1* gene (*SPCA1*$^{-/-}$ cells) because SPCA1 is involved in Mn resistance via its re-delivery into the Golgi apparatus (16,17). Using *SPCA1*$^{-/-}$ cells, which showed extreme sensitivity to high Mn concentrations, we compared six human proteins that are involved in Mn detoxification/efflux. Moreover, we investigated how hZnT10, which belongs to the ZnT transporter family, could mobilize Mn by domain swapping/substitution mutational analyses. These studies provide molecular information of the transporters/channels involved in Mn detoxification/efflux in vertebrate cells.

RESULTS

Characterization of DT40 Cells Deficient in the SPCA1 Gene–We established DT40 cells deficient in the *SPCA1* gene

(*SPCA1*$^{-/-}$) using three KO vectors (Fig. 1*A*) because DT40 cells have trisomic chromosomes 2. *SPCA1*$^{-/-}$ cells did not show any apparent defects in normal culture, but they showed significantly reduced resistance to high Mn concentrations as expected (Fig. 1*B*). Here, the cells failed to grow in the presence of 40 μM $MnSO_4$ or higher concentrations. Consistent with this, *SPCA1*$^{-/-}$ cells failed to efflux Mn out of the cells in the Mn retention assay using radioisotope ^{54}Mn (Fig. 1*C*). Both reduced activities in *SPCA1*$^{-/-}$ cells were completely restored by expression of hSPCA1-GFP (Fig. 1, *B* and *C*), indicating that hSPCA1 has a crucial function in Mn homeostasis by controlling its efflux in DT40 cells. hSPCA1-GFP was localized to the Golgi apparatus in *SPCA1*$^{-/-}$ cells (Fig. 1*D*), indicating that SPCA1 functions by effluxing Mn to the extracellular side via the secretory pathway, as described previously (16,17).

Evaluation of Mn Detoxification/Efflux Protein Functions in SPCA1$^{-/-}$ *cells*–In vertebrates, a number of proteins are involved in Mn detoxification/efflux. We next evaluated these protein functions using *SPCA1*$^{-/-}$ cells by examining restoration of the viability of *SPCA1*$^{-/-}$ cells, stably expressing each of these proteins upon a cytotoxic challenge of increasing Mn concentrations. Specifically, we examined the functions of hFpn, hATP13A1, hATP13A2, hATP13A3, and hZnT10. Fpn locates to the plasma membrane and is indispensable for ferrous iron efflux to the extracellular site, but has also been shown to mobilize Mn (38,39). Expression of hFpn, however, failed to confer resistance to high Mn concentrations in *SPCA1*$^{-/-}$ cells, thus indicating that hFpn does not primarily contribute to Mn detoxification/efflux (Fig. 2*A*). Similarly, we evaluated hATP13A2, which is involved in early-onset parkinsonism, KRS (21), and its homologs hATP13A1 and hATP13A3. We also found that hATP13A1–3 showed virtually no effect on the Mn resistance in *SPCA1*$^{-/-}$ cells to high Mn concentrations in the Alamar Blue assays (Fig. 2*B*). However, a small fraction of the cells cultured at 40 μM $MnSO_4$ appeared morphologically normal by visual observation (data not shown), suggesting that hATP13A1-3 may slightly restore Mn resistance in *SPCA1*$^{-/-}$ cells. We then examined the contribution of hZnT10 to high Mn detoxification. As reported in a complementation assay using a *S. cerevisiae pmr1* mutant (23), hZnT10 completely restored the viability of *SPCA1*$^{-/-}$ cells upon high Mn concentrations (Fig. 2*C*). Consistent with this, hZnT10 decreased accumulated ^{54}Mn in *SPCA1*$^{-/-}$ cells in the Mn retention assay (Fig. 2*D*). Both results indicate that hZnT10 contributes significantly to Mn detoxification. Co-expression of hZnT10 with hSPCA1 conferred greater resistance to high Mn concentrations than that observed for hSPCA1-only expression, and restored resistance to a similar level to that of hZnT10-only expression; the cells survived up to a concentration of 200 μM $MnSO_4$ (Fig. 2*E*). Although we could not examine a reduction of resistance to high Mn concentrations and its restoration by hZnT10 expression in ZnT10-deficient DT40 cells (because DT40 cells do not express *ZnT10* mRNA (data not shown)), these results reiterate the key protective function of hZnT10 against high Mn concentrations. hZnT10 was localized mainly to the Golgi apparatus, but weak immunofluorescent signals were detected in the plasma membrane in *SPCA1*$^{-/-}$ cells (Fig. 2*F*). We closely examined its localization using a surface biotinylation assay with a membrane-impermeable biotinylation reagent and found the biotinylated hZnT10 protein in the cell surface fractions, which confirms that hZnT10 is localized on the cell surface, as reported previously (25) (Fig. 2*G*). However, the current data cannot be used to infer the relative distribution of hZnT10 between the Golgi apparatus and the plasma membrane because hZnT10 was overexpressed under the control of the strong β-actin promoter (30), which limits our ability to determine whether Mn efflux occurred from the plasma membrane or via a secretory pathway through the Golgi. These results, however, indicate that ZnT10, which is the primary transporter protein in excess Mn detoxification, can efflux Mn on the cell surface to the extracellular site.

ZnT10 is Involved in Excess Mn

Detoxification But Not in Excess Zn Detoxification–ZnT10 belongs to the zinc transporter family, but is involved in Mn mobilization for its detoxification. Consequently, we investigated whether hZnT10 is involved in excess Zn detoxification using *ZnT1*$^{-/-}$*MT*$^{-/-}$*ZnT4*$^{-/-}$ cells, which were used previously to evaluate Zn detoxification activity (33,40). Expression of hZnT10 had almost no effects on the resistance of *ZnT1*$^{-/-}$*MT*$^{-/-}$*ZnT4*$^{-/-}$ cells to high Zn concentrations (Fig. 3*A*). Although the Alamar Blue assays showed no contribution to detoxification at a Zn concentration of 60 μM $ZnSO_4$ or higher, visual observation of the cells cultured in the high Zn conditions showed that a small fraction of the cells appeared still morphologically normal (data not shown). To examine metal transport specificity of hZnT10 in more detail, we compared hZnT10 with that of hZnT1 because ZnT1 and ZnT10 can be subdivided into the same subfamily based on sequence similarities (37% identity between hZnT1 and hZnT10) (41,42). Expression of hZnT1 reversed the Zn-sensitive phenotype of *ZnT1*$^{-/-}$*MT*$^{-/-}$*ZnT4*$^{-/-}$ cells, as described previously (33), but failed to confer Mn resistance in *SPCA1*$^{-/-/-}$ cells (Fig. 3*B*). These results clearly showed that expression of hZnT1 or hZnT10 conferred completely different metal resistance in cells. We have not yet examined the cell surface localization of hZnT1 in DT40 cells (30,33), but close examination by immunofluorescence staining and the surface biotinylation assay showed that hZnT1 was localized to the cell surface in both *SPCA1*$^{-/-/-}$ (Fig. 3*C*) and *ZnT1*$^{-/-}$*MT*$^{-/-}$*ZnT4*$^{-/-}$ cells (Fig. 3*D*). The cell surface localization of hZnT10 was confirmed in both cells in parallel studies (Fig. 3, *C* and *D*).

Domain Swapping/Substitution Analysis between hZnT10 and hZnT1–To examine the differences in their metal resistance activity more closely, we constructed domain swapping/substitution mutants between hZnT10 and hZnT1 by considering the unique properties of ZnT10. Specifically, ZnT10 contains an Asn residue instead of a His residue at the conserved position of transmembrane domain (TMD) II, which is thought to form the intramembranous tetrahedral zinc coordination site in other ZnT transporters, including ZnT1 (33,43-48) (Fig. 4). Moreover, ZnT10 has Arg- and Lys-rich sequences in the cytosolic loop between TMDs III and IV, and in the cytosolic C-terminal region; although, the cytosolic loop is known to be rich in His residues in other ZnT transporters (49,50,51). Initially, we expressed the hZnT10 mutants, specifically $hZnT10_{(N43H)}$, $hZnT10_{(hZnT1Cter)}$, or $hZnT10_{(hZnT1Loop)}$ in *SPCA1*$^{-/-/-}$ or *ZnT1*$^{-/-}$*MT*$^{-/-}$*ZnT4*$^{-/-}$ cells, in which the Asn residue in TMD II was substituted with His, the cytosolic C-terminal region or the cytosolic loop between TMDs III and IV was swapped with corresponding regions of hZnT1. We then examined whether these constructs conferred and altered Mn or Zn resistance in *SPCA1*$^{-/-/-}$ or *ZnT1*$^{-/-}$*MT*$^{-/-}$*ZnT4*$^{-/-}$ cells. Expression of $hZnT10_{(hZnT1Cter)}$ and $hZnT10_{(hZnT1Loop)}$ did not alter Mn resistance in *SPCA1*$^{-/-/-}$ cells (Fig. 5, *A* and *C*) or Zn resistance in *ZnT1*$^{-/-}$*MT*$^{-/-}$*ZnT4*$^{-/-}$ cells (Fig. 5, *B* and *D*) when compared with that of hZnT10, indicating that the cytosolic C-terminal region or the cytosolic loop between TMDs III and IV of hZnT1 did not impair Mn transport by hZnT10, and corresponding regions of hZnT10 are not essential for Mn resistance. In contrast, expression of $hZnT10_{(N43H)}$ significantly decreased Mn resistance in *SPCA1*$^{-/-/-}$ cells (Fig. 5*E*) and did not confer Zn resistance in *ZnT1*$^{-/-}$*MT*$^{-/-}$*ZnT4*$^{-/-}$ cells (Fig. 5*F*). The surface biotinylation assay confirmed that all hZnT10 mutants were localized to the cell surface in both *SPCA1*$^{-/-/-}$ (Fig. 5*G*) or *ZnT1*$^{-/-}$*MT*$^{-/-}$*ZnT4*$^{-/-}$ cells (Fig. 5*H*), which excludes the possibility that mislocalization of $hZnT10_{(N43H)}$ in *SPCA1*$^{-/-/-}$ cells resulted in a decrease in Mn resistance, and indicates that the Asn residue in TMD II is extremely important for the Mn transport activity of hZnT10. Taken together, Arg- and Lys-rich sequences in the cytosolic C-terminal region and in the cytosolic loop between TMDs III and IV are not involved in the Mn transport property of hZnT10, whereas the Asn residue in TMD II primarily contributes to Mn transport.

We then constructed the domain swapping/substitution mutants of hZnT1 with

hZnT10 using a similar approach, specifically $hZnT1_{(H43N)}$, $hZnT1_{(hZnT10Cter)}$, and $hZnT1_{(hZnT10Loop)}$, and performed the same experiments. Expression of $hZnT1_{(hZnT10Cter)}$ and $hZnT1_{(hZnT10Loop)}$ did not confer Mn resistance in *SPCA1*$^{-/-}$ cells (Fig. 6, *A* and *C*), and did not alter Zn resistance in *ZnT1*$^{-/-}$*MT*$^{-/-}$*ZnT4*$^{-/-}$ cells (Fig. 6, *B* and *D*), as in the case of hZnT10. Unexpectedly, expression of $hZnT1_{(H43N)}$, however, did confer Mn resistance in *SPCA1*$^{-/-}$ cells (Fig. 6*E*) and the ability to confer Zn resistance in *ZnT1*$^{-/-}$*MT*$^{-/-}$*ZnT4*$^{-/-}$ cells was lost (Fig. 6*F*), indicating that the Asn residue in TMD II can confer Mn transport activity to ZnT1. The surface biotinylation assay confirmed that all hZnT1 mutants were localized at the cell surface in both *SPCA1*$^{-/-}$ (Fig. 6*G*) and *ZnT1*$^{-/-}$*MT*$^{-/-}$*ZnT4*$^{-/-}$ cells (Fig. 6*H*). Taken together, the His-rich clusters in the cytosolic loop between TMDs III and IV of hZnT1 and the cytosolic C-terminal region of hZnT1 are not essential in determining the Zn transport property of hZnT1, while the His residue in TMD II is crucial. Moreover, only substitution of the Asn residue in TMD II is a major determinant of Mn specificity in hZnT1. Moreover, these results reveal that the cytosolic loop between TMDs III and IV and the cytosolic C-terminal region are compatible with each other between hZnT10 and hZnT1 in their Mn or Zn transport activities, despite the presence of several unique differences. The results of Figs. 3, 5, and 6 are summarized in Table 1.

Domain Swapping/Substitution Analysis between hZnT10 and hZnT2–We performed similar swapping/substitution analysis between hZnT10 and hZnT2, using $hZnT2_{(H106N)}$, $hZnT10_{(hZnT2Cter)}$, and $hZnT2_{(hZnT10Cter)}$ mutants. hZnT2 is divided into a different subfamily from hZnT10 and hZnT1, and thus shows only moderate similarity with hZnT10 (28% identity between hZnT10 and hZnT2) (41,42). hZnT2 expression completely reversed the Zn-sensitive phenotypes of *ZnT1*$^{-/-}$*MT*$^{-/-}$*ZnT4*$^{-/-}$ cells (33,40), but unlike $hZnT1_{(H43N)}$, expression of $hZnT2_{(H106N)}$ failed to confer Mn resistance in *SPCA1*$^{-/-}$ cells (Fig. 7*A*). However, the $hZnT2_{(H106N)}$ mutant lost the ability to reverse Zn-sensitive phenotypes of *ZnT1*$^{-/-}$*MT*$^{-/-}$*ZnT4*$^{-/-}$ cells, as observed for the $hZnT1_{(H43N)}$ mutant (Fig. 7*B*). Moreover, the swapping of the cytosolic C-terminal region between hZnT10 and hZnT2 caused these mutants to lose Mn and Zn resistance in *SPCA1*$^{-/-}$ cells and *ZnT1*$^{-/-}$*MT*$^{-/-}$*ZnT4*$^{-/-}$ cells. Specifically, expression of $hZnT10_{(hZnT2Cter)}$ failed to reverse Mn resistance in *SPCA1*$^{-/-}$ cells and that of $hZnT2_{(hZnT10Cter)}$ failed to reverse Zn resistance in *ZnT1*$^{-/-}$*MT*$^{-/-}$*ZnT4*$^{-/-}$ cells (Fig. 7, *C* and *F*). In contrast, expression of $hZnT10_{(hZnT2Cter)}$ did not confer Zn resistance in *ZnT1*$^{-/-}$*MT*$^{-/-}$*ZnT4*$^{-/-}$ cells, whereas that of $hZnT2_{(hZnT10Cter)}$ did not confer Mn resistance in *SPCA1*$^{-/-}$ cells (Fig. 7, *D* and *E*). These results suggest that the cytosolic C-terminal region is not compatible between hZnT10 and hZnT2 in their Mn or Zn transport activity.

We then investigated this incompatibility using complex domain swapping/substitution mutants between hZnT10 and hZnT2 in which all of the three aforementioned features were swapped and substituted. As observed for each mutant between hZnT10 and hZnT2, expression of $hZnT10_{(N43H\text{-}hZnT2Loop\text{-}hZnT2Cter)}$ lost the ability to confer Mn resistance in *SPCA1*$^{-/-}$ cells, whereas that of $hZnT2_{(H106N\text{-}hZnT10Loop\text{-}hZnT10Cter)}$ lost the ability to confer Zn resistance in *ZnT1*$^{-/-}$*MT*$^{-/-}$*ZnT4*$^{-/-}$ cells (Fig. 8, *A* and *D*). Moreover, these swapping/substitutions did not have any effects on the metal substrate specificity between hZnT10 and hZnT2. Expression of $hZnT10_{(N43H\text{-}hZnT2Loop\text{-}hZnT2Cter)}$ did not confer Zn resistance in *ZnT1*$^{-/-}$*MT*$^{-/-}$*ZnT4*$^{-/-}$ cells, and expression of $hZnT2_{(H106N\text{-}hZnT10Loop\text{-}hZnT10Cter)}$ did not confer Mn resistance in *SPCA1*$^{-/-}$ cells (Fig. 8, *B* and *C*). Taken together, unlike the case of hZnT1 and hZnT10, the abovementioned featured domains are incompatible between hZnT10 and hZnT2. The lower similarity of hZnT2 to hZnT10 than hZnT1 to hZnT10 may endow incompatibility with domain swapping/substitutions between hZnT10 and hZnT2. The results of Figs. 7 and 8 are summarized in Table 2.

Residues C52 and L242 in the TMDs II and V *of hZnT10 are Involved in the Control of Metal Substrate Specificity in hZnT10*–Expression of $hZnT10_{(N43H)}$ failed to reverse Zn resistance in *ZnT1*$^{-/-}$*MT*$^{-/-}$*ZnT4*$^{-/-}$ cells despite the fact that reverse substitution

of hZnT1 ($hZnT1_{(H43N)}$) conferred Mn resistance to hZnT1 in the Mn detoxification assay using *SPCA1*$^{-/-}$ cells. This observation indicates that hZnT10 may have a specific mechanism to reduce Zn transport. Finally, we tried to identify specific residues in hZnT10 that are involved in this mechanism. We found that residue C52 in TMD II and L242 in TMD V are present in hZnT10 but not in other hZnT transporters (Fig. 4), and that both residues are thought to be located on the cytosolic side of the putative intramembranous tetrahedral metal coordination site, based on the structure of a bacterial homolog YiiP (42-46). In other hZnT transporters, these positions are predominantly composed of Val, Ile, and Met in TMD II, and Phe in TMD V (Fig. 4). We expressed hZnT10 mutants in *ZnT1*$^{-/-}$*MT*$^{-/-}$*ZnT4*$^{-/-}$ cells, in which the Cys and/or Leu residues were substituted with Val and Phe, respectively, in addition to the N43H substitution ($hZnT10_{(N43H,\ C52V)}$, $hZnT10_{(N43H,\ L242F)}$ and $hZnT10_{(N43H,\ C52V,\ L242F)}$) (Fig. 9, *A*–*C*). Expression of neither $hZnT10_{(N43H,\ C52V)}$ nor $hZnT10_{(N43H,\ L242F)}$ reversed Zn resistance in *ZnT1*$^{-/-}$*MT*$^{-/-}$*ZnT4*$^{-/-}$ cells (Fig. 9, *A* and *B*). However, expression of $hZnT10_{(N43H,\ C52V,\ L242F)}$ moderately restored the ability to confer Zn resistance in *ZnT1*$^{-/-}$*MT*$^{-/-}$*ZnT4*$^{-/-}$ cells (Fig. 9*C*). The cells grew in the presence of 60 μM $ZnSO_4$ but failed to grow in the presence of 80 μM $ZnSO_4$. Moreover, we investigated whether the conferment of Zn resistance by $hZnT10_{(N43H,\ C52V,\ L242F)}$ was facilitated by domain swapping of the cytosolic C-terminal region of hZnT1 with the corresponding region ($hZnT10_{(N43H,\ C52V,\ L242F\text{-}hZnT1Cter)}$). Swapping of the cytosolic C-terminal region did not lead to significant effects (Fig. 9*C*). Consistent with this, expression of $hZnT10_{(N43H\text{-}hZnT1Cter)}$ did not significantly reverse Zn-sensitive phenotypes of *ZnT1*$^{-/-}$*MT*$^{-/-}$*ZnT4*$^{-/-}$ cells (Fig. 9*D*). Last, we examined whether substitution of C52 and L242 with Val and Phe in hZnT10 ($hZnT10_{(C52V,\ L242F)}$) may confer Zn resistance in *ZnT1*$^{-/-}$*MT*$^{-/-}$*ZnT4*$^{-/-}$ cells or impair Mn resistance in *SPCA1*$^{-/-}$ cells. However, these mutations did not confer Zn resistance or impair Mn resistance in the respective cell types (Fig. 9, *E* and *F*). These results indicate that, in addition to the primary role of N43, both C52 in TMD II and L242 in TMD V of hZnT10 are involved in the regulation of metal substrate specificity in hZnT10.

DISCUSSION

Genetic studies using *S. cerevisiae* have contributed significantly to our understanding of Mn metabolism in cells; however, several differences exist between *S. cerevisiae* and vertebrate cells. For example, Ccc1p functions as a major transporter of iron and Mn that is sequestered into vacuoles and thus detoxifies Mn in *S. cerevisiae* (52) but is not identified in vertebrate cells. In contrast, Fpn and ZnT10 are expressed in vertebrate cells but are not present in *S. cerevisiae.* Moreover, in an Mn resistance assay using a *pmr1* mutant of *S. cerevisiae*, extremely high Mn concentrations were required to discriminate Mn resistance (53,54) when compared with those in vertebrate cells. Thus, Mn metabolism should be studied in vertebrate cells. In this study, we compared six human proteins that are involved in Mn detoxification/efflux by using genetically engineered vertebrate cells, *SPCA1*$^{-/-}$ cells, whose extreme sensitivity to high Mn concentrations enabled us to evaluate their contribution to Mn toxicity without directly measuring Mn mobilization.

The Mn detoxification/efflux functions of the evaluated six proteins were examined in different evaluation cell systems and thus their contributions have not yet been directly compared with each other. The present study is important in this aspect because we evaluated the contribution of each protein in the same cell system using *SPCA1*$^{-/-}$ cells. ATP13A proteins, including ATP13A2, are postulated to contribute to Mn detoxification/efflux in both yeast and vertebrate cells when overexpressed (18-20). However, our results indicate that ATP13A proteins have almost no contribution to Mn detoxification/efflux under high Mn conditions. ATP13A2 is suggested to be involved in intracellular Zn homeostasis (55,56), but our re-experiments revealed no contribution of hATP13A2 to conferring Zn resistance in *ZnT1*$^{-/-}$*MT*$^{-/-}$*ZnT4*$^{-/-}$ cells under high Zn concentrations (Nishito, Tsuji and Kambe, unpublished data). Fpn is also

reported to be involved in Mn mobilization (38,39). However, our results indicate that hFpn does not contribute to Mn detoxification/efflux in *SPCA1*$^{-/-}$ cells under high Mn concentrations. In contrast to these proteins, SPCA1 and ZnT10 operate to detoxify/efflux Mn via exporting Mn to an extracellular site in vertebrate cells. Our results indicate that ZnT10 is a primary contributor in the detoxification/efflux of Mn, which may reflect that only mutations to the *ZnT10* gene have been identified as parkinsonism, while mutations of the *SPCA1* gene results in Hailey–Hailey diseases (MIM No. 169600), which is thought to be related to Ca levels and not to disturbances in Mn metabolism (57).

ZnT10 has received much attention because loss of ZnT10 function results in parkinsonism with hypermanganesemia (22,23), despite belonging to ZnT zinc transporters. However, the molecular basis of this condition is missing as well as how ZnT10 recognizes and mobilizes Mn as a transport substrate. Among several characteristic amino acid residues and sequences, we clearly showed that N43 in TMD II plays a critical role for ZnT10 function. Interestingly, hZnT1$_{(H43N)}$ converted hZnT1 from Zn mobilization to Mn mobilization. These results confirmed that the position in TMD II is important for determining the transport metal specificity (42,51), as previously reported using hZnT5 and hZnT8, in which substitution of the His residue with an Asp residue conferred Cd transport activity in addition to Zn (58). The plant MTP8, which transports Mn but not Zn, has an Asp amino acid at this position. MTP8 has four Asp residues, including the Asp residue in TMDs II and V, which are thought to form an intramembranous tetrahedral metal coordination site (59,60). Thus, the finding that the Asn residue at this position of TMD II regulates Mn transport ability is unique, and thus clarification of its specific importance should provide insight into understanding the metal coordination properties in TMDs of ZnT transporters and their homologs. The CDF family of proteins are generally divided into three groups based on their phylogenetic relationships: Zn-CDF, Zn/Fe-CDF, and Mn-CDF (51,61). In this grouping, CDF proteins with the ability to transport Mn, such as MTP8, are classified into the Mn-CDF group, while all of the ZnT transporters are divided into the Zn-CDF family (51,61,62). Thus, careful re-grouping should be performed.

The present study also revealed that the cytosolic loop between TMDs III and IV and the cytosolic C-terminal region are compatible between hZnT1 and hZnT10. This observation is intriguing because the cytosolic C-terminal portion and the cytosolic loop between TMDs III and IV are thought to form a binuclear zinc-binding site allosterically operating for Zn transport activity in a zinc-regulated fashion (43) and likely contribute to a metal substrate determinant (63,64). In contrast to the compatibility between hZnT1 and hZnT10, the domain swapping between hZnT10 and hZnT2 was found to be incompatible. This observation suggests that these regions may be functionally and structurally different among ZnT transporters. However, incompatibility between hZnT10 and hZnT2 may result from their different subcellular localization. Studying and comparing three-dimensional structures of these regions of hZnT10 with those of other hZnT transporters will undoubtedly facilitate answers to this issue.

ZnT10 plays a role in Zn metabolism, locating the early/recycling endosomes or the Golgi apparatus (26,27,65). However, we have no data to show that hZnT10 is involved in the detoxification of high Zn concentrations. Importantly, this study does not completely exclude the possibility that ZnT10 has Zn transport activity and contributes to Zn metabolism because this study was performed under conditions of detoxification/efflux against high Zn concentrations (over 60 μM $ZnSO_4$) using *ZnT1*$^{-/-}$*MT*$^{-/-}$*ZnT4*$^{-/-}$ cells. In support of this idea, overexpression of hZnT5 and hZnT6 failed to confer resistance to *ZnT1*$^{-/-}$*MT*$^{-/-}$*ZnT4*$^{-/-}$ cells in the presence of 60 μM $ZnSO_4$ (Nishito and Kambe, unpublished data). A recent report that the Zn transport function of ZnT10 was accelerated by heterodimer formation with other ZnT transporters, such as ZnT3 (65), suggests that the absence of ZnT transporters in

ZnT1$^{-/-}$*MT*$^{-/-}$*ZnT4*$^{-/-}$ cells may mask the ability of hZnT10 to exert robust Zn transport activity in our evaluation. Because C52 and L242 residues in the TMDs II and V were found to be involved in the regulation of metal substrate specificity in hZnT10, heterodimer formation may affect the conformation of both residues and accessibility of Zn to the intramembranous metal coordination site, which may also change the affinity of N43 towards Zn. Further investigation is required to clarify how ZnT10 contributes to Zn metabolism at the molecular level, as well as its primary function in Mn metabolism.

Because Mn levels are reported to increase in patients of several neurodegenerative diseases (8,14), Mn detoxification/efflux proteins have potential therapeutic functions owing to their ability to decrease Mn accumulation. Thus, the robust Mn detoxification/efflux function of ZnT10 may be important against these pathologies. The present results contribute to providing clues that should facilitate Mn transport activity of ZnT10 in a specific manner, as well as information that aids our understanding of the relationship between Mn and Zn metabolic systems.

EXPERIMENTAL PROCEDURES

Cell Culture and Transfection–Chicken B lymphocyte-derived DT40 cells were maintained in RPMI 1640 (Nacalai Tesque, Kyoto, Japan) supplemented with 10% heat-inactivated fetal calf serum (Multiser, Trace Scientific, Melbourne, Australia), 1% chicken serum (Invitrogen, Carlsbad, CA) and 50 μM 2-mercaptoethanol (Sigma, St. Louis, MO) at 39.5 °C, as described previously (31). DNA transfection into DT40 cells was carried out using electroporation, as described previously (31). DT40 cells deficient in the *SPCA1* gene (*SPCA1*$^{-/-}$ cells) were established using three KO vectors shown in Fig. 1*A*. Southern and northern blot analysis was performed as described previously (32). Genomic DNA (20 μg) prepared from DT40 cells or 20 μg total RNA extracted from the cells using Sepasol I (Nacalai Tesque) was used. Radioimages were obtained using a FLA5000 Bio imaging analyzer (Fujifilm, Tokyo, Japan). More than three independent clones were established per disruptants and transfectants. *ZnT1*$^{-/-}$*MT*$^{-/-}$*ZnT4*$^{-/-}$ cells have been established and reported previously (33).

Plasmid Construction–Plasmids used for the expression of C-terminally GFP-tagged hSPCA1 (hSPCA1-GFP) (15), N-terminally FLAG-tagged hATP13A1 (FLAG-hATP13A1), C-terminally HA-tagged hATP13A2 (hATP13A2-HA), N-terminally HA-tagged hATP13A3 (HA-hATP13A3), C-terminally HA tagged hZnT10 (hZnT10-HA), N-terminally Myc-tagged hZnT10 (Myc-hZnT10), N-terminally FLAG-tagged hZnT1 (FLAG-hZnT1), or C-terminally HA tagged hZnT2 (hZnT2-HA) were constructed by inserting each cDNA into pA-Puro or pA-Zeocin vectors (34). The truncated forms of h*ATP13A1* and h*ATP13A3* cDNAs were purchased from DNAFORM (http://www.dnaform.jp/ja/) and their full-length forms were prepared by ligating them with the lacking fragments of RT-PCR-amplified h*ATP13A1* or h*ATP13A3* cDNA. The hATP13A2-HA was constructed by replacing a V5-His tag (21) with the HA tag, or the hZnT10-HA was constructed by fusing hZnT10 (23) with the HA tag. The hFpn gene, which is fused with the C-terminally V5 tag, was described previously (35). All cDNAs constructed here were sequenced in both directions. The KO vectors used for disruption of the *SPCA1* gene were constructed using the amplified genomic DNA fragments with gene-specific primers by KOD-FX polymerase (Toyobo, Osaka Japan), as described previously (31). All plasmids were linearized with appropriate restriction enzymes prior to electroporation.

Cytotoxicity Assay Against High Mn or Zn Concentrations–DT40 cells were inoculated at a density of 10×10^4 cells/mL in 96-well plates and treated with $MnSO_4$ or $ZnSO_4$ at the indicated concentrations for 2 d. Alamar Blue reagent (AbD Serotec, Ltd., Oxford, UK) was then added to the culture media and incubated for 3–4 h. The absorbance in the medium was measured at 570 and 600 nm using PowerScan 4 (DS Pharma Biomedical, Osaka, Japan), according

to the protocol of the manufacturer.

Measurement of Mn Transport Activity–DT40 cells were cultured in 6-well plates and 1 μM [^{54}Mn]-labeled $MnCl_2$ (PerkinElmer, Boston, MA) was added to the culture media in all wells. After 24 h, the cells were washed twice with ice-cold culture medium and suspended in phosphate-buffered saline (PBS) containing 0.05% EDTA. The radioactivity of ^{54}Mn was measured using an auto-well gamma counter (Wizard^2; PerkinElmer Japan, Kanagawa, Japan) and data normalized by the total cellular protein. Data are depicted as mean ± SD. Statistical significance was determined by the Student's *t* test and accepted at $p < 0.01$.

Generation of Anti-hZnT10 and Anti-hZnT1 Monoclonal Antibodies–Fused proteins consisting of the cytosolic carboxyl terminal portion of hZnT10 (95 residues from Leu^{391} to stop codon) and maltose binding protein, or the cytosolic carboxyl terminal portion of hZnT1 (167 residues from Leu^{341} to stop codon) and maltose binding protein were used as antigens. The anti-hZnT10 or anti-hZnT1 monoclonal antibody was produced as described previously (36,37). An ascites was generated by injection of 1×10^7 hybridoma cells into pristine-primed mice.

Immunoblotting–Immunoblotting was performed as described previously (30). Briefly, the blotted PVDF membrane (Immobilon-P, Millipore Corp., Bedford, MA) was blocked with a solution of 5% skimmed milk and 0.1% Tween-20 in PBS prior to incubation with anti-FLAG M2 (1:3,000, Sigma, F3165), anti-HA HA-11 (1:3,000, Covance, Emeryville, CA, MMS-101P), anti-Myc (1:3,000, Santa Cruz Biotechnology Inc., sc-40) anti-V5 (1:3,000, Nacalai Tesque, 04434-94), anti-ZnT10 (1:3,000), anti-ZnT1 (1:3,000), anti-GFP (1:1,000, Invitrogen, G10362), anti-tubulin, (1:10,000, Sigma, T7816), anti-calnexin (1:10,000, Enzo Life Sciences, ADI-SPA-860), or anti-chicken IgM M4 (1:3,000, Southern Biotech, 8300-01) antibodies in blocking solution. Horseradish peroxidase-conjugated anti-mouse or rabbit secondary antibodies (GE Healthcare, Waukesha, WI, NA931 or NA934) were added at a 1:3,000 dilution for detection. The fluoro-image was obtained using a LAS1000 plus (Fujifilm, Tokyo, Japan) or a LAS 500 (GE Healthcare).

Cell Surface Biotinylation Assay–Cells stably expressing WT or mutant hZnT10 or hZnT1 were washed twice with ice-cold PBS and then EZ-Link, a sulfo-NHS-SS-biotin reagent (Pierce Protein Biology, ThermoFisher Scientific) was used to biotinylate lysine residues exposed on the extracellular surface. Biotinylated proteins were recovered from streptavidin-coupled beads in 6× SDS sample buffer and then immunoblotted.

Immunofluorescence Staining–Double immunostaining for tagged proteins used in this study and GM130 was performed as described previously (30). Briefly, the cells were stained with an anti-HA tag polyclonal antibody (1:500, MBL, 561), an anti-FLAG tag polyclonal antibody (anti-DDDDK; 1:500, MBL, PM020), anti-GFP (1:50, Invitrogen, G10362) or anti-GM130 (1:100, BD Transduction Laboratories, G65120), followed by goat anti-mouse IgG conjugated to Alexa 594 (Molecular Probes, A11032) or donkey anti-rabbit IgG conjugated to Alexa 488 (Molecular Probes, A21206) as the secondary antibodies. The stained cells were observed using a Zeiss Axioplan 2 microscope equipped with an Olympus digital camera (Metamorph, Olympus, Tokyo, Japan) or a fluorescent microscope FSX100 (Olympus). Images were analyzed using Adobe Photoshop Elements (Adobe Systems Inc., San Jose, CA).

Acknowledgments: We thank Dr. Christian Kubisch (University Medical Center Hamburg-Eppendorf, Hamburg, Germany) for providing the hATP13A2-V5-His plasmid. This work was supported by Grants-in-Aid for Young Scientists (B), Challenging Exploratory Research and Scientific Research (B) from the Japan Society for the Promotion of Science (KAKENHI, Grant Nos. 21780309, 26660086, and 15H04501), the Fuji Foundation for Protein Research, the Salt Science Research Foundation, the Kato Memorial Bioscience Foundation, the

Sasakawa Scientific Research Grant from the Japan Science Society, and the Mochida Memorial Foundation for Medical and Pharmaceutical Research (to T. K.).

Conflict of interest: The authors declare that they have no conflict of interest with the contents of this article.

Author contributions: YN performed the experiments, analyzed and interpreted the data, and co-wrote the manuscript. NT, TT, TY, and FT performed the experiments and analyzed the data. HF and SH performed the Mn retention assay and contributed to the concept. FO, AM, and HN generated antibodies. KT, RR, SK, and HM cloned genes and contributed to the concept. TK directed the project, designed and performed the experiments, analyzed and interpreted the data, and wrote the manuscript. All authors reviewed the manuscript.

REFERENCES

1. Aschner, J. L., and Aschner, M. (2005) Nutritional aspects of manganese homeostasis. *Mol. Aspects Med.* **26**, 353–362
2. Wood, R. J. (2009) Manganese and birth outcome. *Nutr. Rev.* **67**, 416–420
3. Aschner, M., Erikson, K. M., Herrero Hernandez, E., and Tjalkens, R. (2009) Manganese and its role in Parkinson's disease: from transport to neuropathology. *Neuromolecular Med.* **11**, 252–266
4. Lucchini, R. G., Martin, C. J., and Doney, B. C. (2009) From manganism to manganese-induced parkinsonism: a conceptual model based on the evolution of exposure. *Neuromolecular Med.* **11**, 311–321
5. Culotta, V. C., Yang, M., and Hall, M. D. (2005) Manganese transport and trafficking: lessons learned from *Saccharomyces cerevisiae*. *Eukaryot. Cell* **4**, 1159–1165
6. Reddi, A. R., Jensen, L. T., and Culotta, V. C. (2009) Manganese homeostasis in *Saccharomyces cerevisiae*. *Chem. Rev.* **109**, 4722–4732
7. Au, C., Benedetto, A., and Aschner, M. (2008) Manganese transport in eukaryotes: the role of DMT1. *Neurotoxicology* **29**, 569–576
8. Bowman, A. B., Kwakye, G. F., Hernandez, E. H., and Aschner, M. (2011) Role of manganese in neurodegenerative diseases. *J. Trace. Elem. Med. Biol.* **25**, 191–203
9. Fujishiro, H., Yano, Y., Takada, Y., Tanihara, M., and Himeno, S. (2012) Roles of ZIP8, ZIP14, and DMT1 in transport of cadmium and manganese in mouse kidney proximal tubule cells. *Metallomics* **4**, 700–708
10. Fujishiro, H., Ohashi, T., Takuma, M., and Himeno, S. (2013) Suppression of ZIP8 expression is a common feature of cadmium-resistant and manganese-resistant RBL-2H3 cells. *Metallomics* **5**, 437–444

11. Jenkitkasemwong, S., Wang, C. Y., Mackenzie, B., and Knutson, M. D. (2012) Physiologic implications of metal-ion transport by ZIP14 and ZIP8. *Biometals* **25**, 643–655
12. Jabado, N., Jankowski, A., Dougaparsad, S., Picard, V., Grinstein, S., and Gros, P. (2000) Natural resistance to intracellular infections: natural resistance-associated macrophage protein 1 (Nramp1) functions as a pH-dependent manganese transporter at the phagosomal membrane. *J. Exp. Med.* **192**, 1237–1248
13. Chen, P., Chakraborty, S., Mukhopadhyay, S., Lee, E., Paoliello, M. M., Bowman, A. B., and Aschner, M. (2015) Manganese homeostasis in the nervous system. *J. Neurochem.* **134**, 601–610
14. Hozumi, I., Hasegawa, T., Honda, A., Ozawa, K., Hayashi, Y., Hashimoto, K., Yamada, M., Koumura, A., Sakurai, T., Kimura, A., Tanaka, Y., Satoh, M., and Inuzuka, T. (2011) Patterns of levels of biological metals in CSF differ among neurodegenerative diseases. *J. Neurol. Sci.* **303**, 95–99
15. Ton, V. K., Mandal, D., Vahadji, C., and Rao, R. (2002) Functional expression in yeast of the human secretory pathway Ca^{2+}, Mn^{2+}-ATPase defective in Hailey-Hailey disease. *J. Biol. Chem.* **277**, 6422–6427
16. Mukhopadhyay, S., and Linstedt, A. D. (2011) Identification of a gain-of-function mutation in a Golgi P-type ATPase that enhances Mn^{2+} efflux and protects against toxicity. *Proc. Natl. Acad. Sci. U S A.* **108**, 858–863
17. Leitch, S., Feng, M., Muend, S., Braiterman, L. T., Hubbard, A. L., and Rao, R. (2011) Vesicular distribution of Secretory Pathway Ca^{2+}-ATPase isoform 1 and a role in manganese detoxification in liver-derived polarized cells. *Biometals* **24**, 159-170
18. Tan, J., Zhang, T., Jiang, L., Chi, J., Hu, D., Pan, Q., Wang, D., and Zhang, Z. (2011) Regulation of intracellular manganese homeostasis by Kufor-Rakeb syndrome-associated ATP13A2 protein. *J. Biol. Chem.* **286**, 29654–29662
19. Gitler, A. D., Chesi, A., Geddie, M. L., Strathearn, K. E., Hamamichi, S., Hill, K. J., Caldwell, K. A., Caldwell, G. A., Cooper, A. A., Rochet, J. C., and Lindquist, S. (2009) Alpha-synuclein is part of a diverse and highly conserved interaction network that includes PARK9 and manganese toxicity. *Nat. Genet.* **41**, 308–315
20. Chesi, A., Kilaru, A., Fang, X., Cooper, A. A., and Gitler, A. D. (2012) The role of the Parkinson's disease gene PARK9 in essential cellular pathways and the manganese homeostasis network in yeast. *PLoS One* **7**, e34178

21. Ramirez, A., Heimbach, A., Grundemann, J., Stiller, B., Hampshire, D., Cid, L. P., Goebel, I., Mubaidin, A. F., Wriekat, A. L., Roeper, J., Al-Din, A., Hillmer, A. M., Karsak, M., Liss, B., Woods, C. G., Behrens, M. I., and Kubisch, C. (2006) Hereditary parkinsonism with dementia is caused by mutations in ATP13A2, encoding a lysosomal type 5 P-type ATPase. *Nat. Genet.* **38**, 1184–1191

22. Quadri, M., Federico, A., Zhao, T., Breedveld, G. J., Battisti, C., Delnooz, C., Severijnen, L. A., Di Toro Mammarella, L., Mignarri, A., Monti, L., Sanna, A., Lu, P., Punzo, F., Cossu, G., Willemsen, R., Rasi, F., Oostra, B. A., van de Warrenburg, B. P., and Bonifati, V. (2012) Mutations in SLC30A10 cause parkinsonism and dystonia with hypermanganesemia, polycythemia, and chronic liver disease. *Am. J. Hum. Genet.* **90**, 467–477

23. Tuschl, K., Clayton, P. T., Gospe, S. M., Jr., Gulab, S., Ibrahim, S., Singhi, P., Aulakh, R., Ribeiro, R. T., Barsottini, O. G., Zaki, M. S., Del Rosario, M. L., Dyack, S., Price, V., Rideout, A., Gordon, K., Wevers, R. A., Chong, W. K., and Mills, P. B. (2012) Syndrome of hepatic cirrhosis, dystonia, polycythemia, and hypermanganesemia caused by mutations in SLC30A10, a manganese transporter in man. *Am. J. Hum. Genet.* **90**, 457–466

24. Ng, E., Lind, P. M., Lindgren, C., Ingelsson, E., Mahajan, A., Morris, A., and Lind, L. (2015) Genome-wide association study of toxic metals and trace elements reveals novel associations. *Hum. Mol. Genet.* **24**, 4739–4745

25. Leyva-Illades, D., Chen, P., Zogzas, C. E., Hutchens, S., Mercado, J. M., Swaim, C. D., Morrisett, R. A., Bowman, A. B., Aschner, M., and Mukhopadhyay, S. (2014) SLC30A10 is a cell surface-localized manganese efflux transporter, and parkinsonism-causing mutations block its intracellular trafficking and efflux activity. *J. Neurosci.* **34**, 14079–14095

26. Bosomworth, H. J., Thornton, J. K., Coneyworth, L. J., Ford, D., and Valentine, R. A. (2012) Efflux function, tissue-specific expression and intracellular trafficking of the Zn transporter ZnT10 indicate roles in adult Zn homeostasis. *Metallomics* **4**, 771–779

27. Patrushev, N., Seidel-Rogol, B., and Salazar, G. (2012) Angiotensin II Requires Zinc and Downregulation of the Zinc Transporters ZnT3 and ZnT10 to Induce Senescence of Vascular Smooth Muscle Cells. *PLoS One* **7**, e33211

28. Suzuki, T., Ishihara, K., Migaki, H., Matsuura, W., Kohda, A., Okumura, K., Nagao, M., Yamaguchi-Iwai, Y., and Kambe, T. (2005) Zinc transporters, ZnT5 and ZnT7, are

required for the activation of alkaline phosphatases, zinc-requiring enzymes that are glycosylphosphatidylinositol-anchored to the cytoplasmic membrane. *J. Biol. Chem.* **280**, 637–643

29. Ishihara, K., Yamazaki, T., Ishida, Y., Suzuki, T., Oda, K., Nagao, M., Yamaguchi-Iwai, Y., and Kambe, T. (2006) Zinc transport complexes contribute to the homeostatic maintenance of secretory pathway function in vertebrate cells. *J. Biol. Chem.* **281**, 17743–17750
30. Fukunaka, A., Kurokawa, Y., Teranishi, F., Sekler, I., Oda, K., Ackland, M. L., Faundez, V., Hiromura, M., Masuda, S., Nagao, M., Enomoto, S., and Kambe, T. (2011) Tissue Nonspecific Alkaline Phosphatase Is Activated via a Two-step Mechanism by Zinc Transport Complexes in the Early Secretory Pathway. *J. Biol. Chem.* **286**, 16363–16373
31. Kambe, T. (2014) Methods to Evaluate Zinc Transport into and out of the Secretory and Endosomal-Lysosomal Compartments in DT40 Cells. *Methods Enzymol.* **534**, 77–92
32. Matsuura, W., Yamazaki, T., Yamaguchi-Iwai, Y., Masuda, S., Nagao, M., Andrews, G. K., and Kambe, T. (2009) SLC39A9 (ZIP9) regulates zinc homeostasis in the secretory pathway: characterization of the ZIP subfamily I protein in vertebrate cells. *Biosci. Biotechnol. Biochem.* **73**, 1142–1148
33. Fujimoto, S., Itsumura, N., Tsuji, T., Anan, Y., Tsuji, N., Ogra, Y., Kimura, T., Miyamae, Y., Masuda, S., Nagao, M., and Kambe, T. (2013) Cooperative Functions of ZnT1, Metallothionein and ZnT4 in the Cytoplasm Are Required for Full Activation of TNAP in the Early Secretory Pathway. *PLoS One* **8**, e77445
34. Suzuki, T., Ishihara, K., Migaki, H., Nagao, M., Yamaguchi-Iwai, Y., and Kambe, T. (2005) Two different zinc transport complexes of cation diffusion facilitator proteins localized in the secretory pathway operate to activate alkaline phosphatases in vertebrate cells. *J. Biol. Chem.* **280**, 30956–30962
35. Kono, S., Yoshida, K., Tomosugi, N., Terada, T., Hamaya, Y., Kanaoka, S., and Miyajima, H. (2010) Biological effects of mutant ceruloplasmin on hepcidin-mediated internalization of ferroportin. *Biochim. Biophys. Acta* **1802**, 968–975
36. Kambe, T., Narita, H., Yamaguchi-Iwai, Y., Hirose, J., Amano, T., Sugiura, N., Sasaki, R., Mori, K., Iwanaga, T., and Nagao, M. (2002) Cloning and characterization of a novel mammalian zinc transporter, zinc transporter 5, abundantly expressed in pancreatic beta cells. *J. Biol. Chem.* **277**, 19049–19055.

37. Hashimoto, A., Ohkura, K., Takahashi, M., Kizu, K., Narita, H., Enomoto, S., Miyamae, Y., Masuda, S., Nagao, M., Irie, K., Ohigashi, H., Andrews, G. K., and Kambe, T. (2015) Soybean extracts increase cell surface ZIP4 abundance and cellular zinc levels: a potential novel strategy to enhance zinc absorption by ZIP4 targeting. *Biochem. J.* **472**, 183–193

38. Yin, Z., Jiang, H., Lee, E. S., Ni, M., Erikson, K. M., Milatovic, D., Bowman, A. B., and Aschner, M. (2010) Ferroportin is a manganese-responsive protein that decreases manganese cytotoxicity and accumulation. *J. Neurochem.* **112**, 1190–1198

39. Madejczyk, M. S., and Ballatori, N. (2012) The iron transporter ferroportin can also function as a manganese exporter. *Biochim. Biophys. Acta.* **1818**, 651–657

40. Itsumura, N., Inamo, Y., Okazaki, F., Teranishi, F., Narita, H., Kambe, T., and Kodama, H. (2013) Compound Heterozygous Mutations in SLC30A2/ZnT2 Results in Low Milk Zinc Concentrations: A Novel Mechanism for Zinc Deficiency in a Breast-Fed Infant. *PLoS One* **8**, e64045

41. Kambe, T., Suzuki, T., Nagao, M., and Yamaguchi-Iwai, Y. (2006) Sequence similarity and functional relationship among eukaryotic ZIP and CDF transporters. *Genomics Proteomics Bioinformatics* **4**, 1–9

42. Kambe, T. (2012) Molecular Architecture and Function of ZnT Transporters. *Curr. Top. Membr.* **69**, 199-220

43. Lu, M., and Fu, D. (2007) Structure of the zinc transporter YiiP. *Science* **317**, 1746–1748

44. Lu, M., Chai, J., and Fu, D. (2009) Structural basis for autoregulation of the zinc transporter YiiP. *Nat. Struct. Mol. Biol.* **16**, 1063–1067

45. Gupta, S., Chai, J., Cheng, J., D'Mello, R., Chance, M. R., and Fu, D. (2014) Visualizing the kinetic power stroke that drives proton-coupled zinc(II) transport. *Nature* **512**, 101-104

46. Coudray, N., Valvo, S., Hu, M., Lasala, R., Kim, C., Vink, M., Zhou, M., Provasi, D., Filizola, M., Tao, J., Fang, J., Penczek, P. A., Ubarretxena-Belandia, I., and Stokes, D. L. (2013) Inward-facing conformation of the zinc transporter YiiP revealed by cryoelectron microscopy. *Proc. Natl. Acad. Sci. U S A.* **110**, 2140–2145

47. Shusterman, E., Beharier, O., Shiri, L., Zarivach, R., Etzion, Y., Campbell, C. R., Lee, I. H., Okabayashi, K., Dinudom, A., Cook, D. I., Katz, A., and Moran, A. (2014) ZnT-1

extrudes zinc from mammalian cells functioning as a Zn^{2+}/H^{+} exchanger. *Metallomics* **6**, 1656–1663

48. Ohana, E., Hoch, E., Keasar, C., Kambe, T., Yifrach, O., Hershfinkel, M., and Sekler, I. (2009) Identification of the Zn^{2+} binding site and mode of operation of a mammalian Zn2+ transporter. *J. Biol. Chem.* **284**, 17677–17686
49. Seve, M., Chimienti, F., Devergnas, S., and Favier, A. (2004) In silico identification and expression of SLC30 family genes: an expressed sequence tag data mining strategy for the characterization of zinc transporters' tissue expression. *BMC Genomics* **5**, 32
50. Fukada, T., and Kambe, T. (2011) Molecular and genetic features of zinc transporters in physiology and pathogenesis. *Metallomics* **3**, 662–674
51. Kambe, T., Tsuji, T., Hashimoto, A., and Itsumura, N. (2015) The Physiological, Biochemical, and Molecular Roles of Zinc Transporters in Zinc Homeostasis and Metabolism. *Physiol. Rev.* **95**, 749–784
52. Lapinskas, P. J., Lin, S. J., and Culotta, V. C. (1996) The role of the *Saccharomyces cerevisiae CCC1* gene in the homeostasis of manganese ions. *Mol. Microbiol.* **21**, 519–528
53. Lin, S. J., and Culotta, V. C. (1996) Suppression of oxidative damage by *Saccharomyces cerevisiae ATX2*, which encodes a manganese-trafficking protein that localizes to Golgi-like vesicles. *Mol. Cell. Biol.* **16**, 6303–6312
54. Wei, Y., Chen, J., Rosas, G., Tompkins, D. A., Holt, P. A., and Rao, R. (2000) Phenotypic screening of mutations in Pmr1, the yeast secretory pathway Ca^{2+}/Mn^{2+}-ATPase, reveals residues critical for ion selectivity and transport. *J. Biol. Chem.* **275**, 23927–23932
55. Park, J. S., Koentjoro, B., Veivers, D., Mackay-Sim, A., and Sue, C. M. (2014) Parkinson's disease-associated human ATP13A2 (PARK9) deficiency causes zinc dyshomeostasis and mitochondrial dysfunction. *Hum. Mol. Genet.* **23**, 2802–2815
56. Tsunemi, T., and Krainc, D. (2014) Zn^{2+} dyshomeostasis caused by loss of ATP13A2/PARK9 leads to lysosomal dysfunction and alpha-synuclein accumulation. *Hum. Mol. Genet.* **23**, 2791–2801
57. Aronchik, I., Behne, M. J., Leypoldt, L., Crumrine, D., Epstein, E., Ikeda, S., Mizoguchi, M., Bench, G., Pozzan, T., and Mauro, T. (2003) Actin reorganization is abnormal and cellular ATP is decreased in Hailey-Hailey keratinocytes. *J. Invest. Dermatol.* **121**, 681–687

58. Hoch, E., Lin, W., Chai, J., Hershfinkel, M., Fu, D., and Sekler, I. (2012) Histidine pairing at the metal transport site of mammalian ZnT transporters controls Zn^{2+} over Cd^{2+} selectivity. *Proc. Natl. Acad. Sci. U S A.* **109**, 7202–7207

59. Delhaize, E., Kataoka, T., Hebb, D. M., White, R. G., and Ryan, P. R. (2003) Genes encoding proteins of the cation diffusion facilitator family that confer manganese tolerance. *Plant Cell* **15**, 1131–1142

60. Pedas, P., Schiller Stokholm, M., Hegelund, J. N., Ladegard, A. H., Schjoerring, J. K., and Husted, S. (2014) Golgi localized barley MTP8 proteins facilitate Mn transport. *PLoS One* **9**, e113759

61. Montanini, B., Blaudez, D., Jeandroz, S., Sanders, D., and Chalot, M. (2007) Phylogenetic and functional analysis of the Cation Diffusion Facilitator (CDF) family: improved signature and prediction of substrate specificity. *BMC Genomics* **8**, 107

62. Gustin, J. L., Zanis, M. J., and Salt, D. E. (2011) Structure and evolution of the plant cation diffusion facilitator family of ion transporters. *BMC Evol. Biol.* **11**, 76

63. Kawachi, M., Kobae, Y., Mimura, T., and Maeshima, M. (2008) Deletion of a histidine-rich loop of AtMTP1, a vacuolar Zn^{2+}/H^{+} antiporter of Arabidopsis thaliana, stimulates the transport activity. *J. Biol. Chem.* **283**, 8374–8383

64. Blindauer, C. A., and Schmid, R. (2010) Cytosolic metal handling in plants: determinants for zinc specificity in metal transporters and metallothioneins. *Metallomics* **2**, 510–529

65. Zhao, Y., Feresin, R. G., Falcon-Perez, J. M., and Salazar, G. (2016) Differential Targeting of SLC30A10/ZnT10 Heterodimers to Endolysosomal Compartments Modulates EGF-induced MEK/ERK1/2 Activity. *Traffic* **17,** 267–288

FOOTNOTES

The abbreviations used are: Mn, manganese; Zn, zinc; Ca, calcium; SPCA, secretory pathway calcium channel; ZnT, zinc transporter; TMD, transmembrane domain.

FIGURE LEGENDS

Figure 1. *SPCA1*$^{-/-}$ cells show significantly reduced resistance to high Mn concentrations. ***A***, targeted disruption of the c*SPCA1* gene. Three targeting constructs were designed to disrupt the exon encoding actuator domain. The *HisD*, *Bsr*, or *Puro* drug-resistant marker cassettes were flanked by mutated loxP sites indicated by gray arrowheads. Gray boxes indicate the position of 5′ and 3′ probes. Southern blot (*right upper* panels) and northern blot (*right bottom* panel) analyses confirmed the disruption of the *SPCA1* gene. ***B***, *SPCA1*$^{-/-}$ cells were significantly sensitive to high Mn concentrations. Cells were grown in the presence of the indicated concentrations of $MnSO_4$ for 2 d and the number of living cells was counted (*left*

graph), and evaluated by the Alamar Blue assay (*right* graph). Relative values are plotted as a percentage of living cells without $MnSO_4$ for each group of cells. The growth curves of wild-type (WT), *SPCA1*$^{-/-}$, and *SPCA1*$^{-/-}$ stably expressing hSPCA1-GFP are shown. Each experiment was performed at least three times. Note that hSPCA1-GFP expression reversed the phenotypes of *SPCA1*$^{-/-}$ cells. ***C***, *SPCA1*$^{-/-}$ cells accumulated high Mn concentrations in the cells. Amounts of Mn in the cells were evaluated by measuring ^{54}Mn accumulated in the cells cultured for 24 h in the presence of 10 μM $^{54}MnCl_2$. Each value is the mean ± SD of three independent experiments (**P* < 0.01). Note that hSPCA1-GFP expression decreased the accumulation of ^{54}Mn in *SPCA1*$^{-/-}$ cells, although the level of accumulated ^{54}Mn in the cells at 24 h does not necessarily reflect steady state levels of cellular Mn. ***D***, the subcellular localization of hSPCA1 expressed in *SPCA1*$^{-/-}$ cells. hSPCA1-GFP (green), GM130 (red), and the merged images are shown. Confirmation of stable hSPCA1-GFP expression in *SPCA1*$^{-/-}$ cells by immunoblotting. Ten micrograms of total cellular protein was loaded onto each lane, and the same membrane was used for detection of both hSPCA1 and tubulin. Tubulin is shown as a loading control.

Figure 2. Evaluation of the conferment of Mn detoxification using *SPCA1*$^{-/-}$ cells. ***A***, hFpn failed to reverse the phenotypes of *SPCA1*$^{-/-}$ cells. The growth curves of wild-type (WT), *SPCA1*$^{-/-}$, *SPCA1*$^{-/-}$ stably expressing hSPCA1-GFP, and *SPCA1*$^{-/-}$ stably expressing hFpn-V5 are shown. Confirmation of stable hFpn and hSPCA1 expression in *SPCA1*$^{-/-}$ cells by immunoblotting (*lower* panels). ***B***, hATP13A1, hATP13A2, and hATP13A3 had almost no effects on Mn resistance in *SPCA1*$^{-/-}$ cells. The growth curves of wild-type (WT), *SPCA1*$^{-/-}$, *SPCA1*$^{-/-}$ stably expressing FLAG-hATP13A1, hATP13A2-HA, or HA-hATP13A3 are shown. Confirmation of stable expression of hATP13A1, hATP13A2, and hATP13A3 in *SPCA1*$^{-/-}$ cells by immunoblotting (*lower* panels). ***C***, hZnT10 completely reversed the phenotypes of *SPCA1*$^{-/-}$ cells. The growth curves of wild-type (WT), *SPCA1*$^{-/-}$, and *SPCA1*$^{-/-}$ stably expressing hZnT10-HA are shown. Confirmation of stable hZnT10 expression in *SPCA1*$^{-/-}$ cells by immunoblotting (*lower* panels). ***D***, hZnT10 decreased accumulated ^{54}Mn in *SPCA1*$^{-/-}$ cells. Amounts of accumulated ^{54}Mn in the cells at 24 h were evaluated as in Fig. 1***C***. Each value is the mean ± SD of three independent experiments (**P* < 0.01). ***E***, co-expression of hZnT10 with hSPCA1 conferred more resistance to high Mn concentrations than that of single expression of hSPCA1. The growth curves of wild-type (WT), *SPCA1*$^{-/-}$, *SPCA1*$^{-/-}$ stably expressing hZnT10, *SPCA1*$^{-/-}$ stably expressing hSPCA1, and *SPCA1*$^{-/-}$ stably expressing both hZnT10 and hSPCA1 are shown. Confirmation of stable hZnT10 and hSPCA1 expression in *SPCA1*$^{-/-}$ cells by immunoblotting (*lower* panels). Note that co-expression of hZnT10 with hSPCA1 conferred greater resistance to high Mn concentrations compared with that of only hSPCA1 expression. ***F***, immunofluorescence staining of hZnT10 expressed in *SPCA1*$^{-/-}$ cells. hZnT10 (green), GM130 (red), and the merged images are shown. ***G***, the cell surface localization of hZnT10 evaluated by the surface biotinylation assay. Cells treated with the biotinylation reagent (sulfo-NHS-SS-biotin) were solubilized and the biotinylated protein was then captured using streptavidin beads and analyzed by immunoblot analysis. Input refers to aliquots of the biotinylated proteins before avidin capture (*i.e.*, total cell lysate), while biotinylation refers to avidin-captured proteins. Tubulin and IgM were used as loading controls for input and biotinylation, respectively. The representative results of three independent experiments are displayed. In (***A***)–(***C***) and (***E***), cells were grown in the presence of the indicated concentrations of $MnSO_4$ for 2 d and the numbers of living cells were evaluated by the Alamar Blue assay at least three times. Tubulin and calnexin are shown as the loading controls.

Figure 3. ZnT10 is involved in Mn transport rather than Zn transport. ***A***, expression of hZnT10 did not restore Zn resistance of *ZnT1*$^{-/-}$*MT*$^{-/-}$*ZnT4*$^{-/-}$ cells. Cells stably expressing hZnT10 or hZnT1 were grown in the presence of the indicated concentrations of $ZnSO_4$ for 2 d

and the numbers of living cells were evaluated by the Alamar Blue assay. Confirmation of stable hZnT10 or hZnT1 expression in *ZnT1*$^{-/-}$*MT*$^{-/-}$*ZnT4*$^{-/-}$ cells by immunoblotting (*lower* panels). ***B***, expression of hZnT1 failed to confer Mn resistance of *SPCA1*$^{-/-/-}$ cells. Cells stably expressing hZnT1 or hZnT10 were grown in the presence of the indicated concentrations of $MnSO_4$ for 2 d and the number of living cells were evaluated by the Alamar Blue assay. Confirmation of stable hZnT10 or hZnT1 expression in *SPCA1*$^{-/-/-}$ cells by immunoblotting (*lower* panels). In (***A***) and (***B***), the Alamar Blue assay was performed at least three times. Calnexin is shown as the loading controls. ***C***, the plasma membrane localization of hZnT1 and hZnT10 expressed in *SPCA1*$^{-/-/-}$cells are shown. Immunofluorescence staining of both proteins was performed as presented Fig. 2***F*** (*left* part). The biotinylation assay was performed as in Fig. 2***G*** (*right* part). ***D***, the plasma membrane localization of hZnT1 and hZnT10 expressed in *ZnT1*$^{-/-}$*MT*$^{-/-}$*ZnT4*$^{-/-}$ cells are shown. Immunofluorescence staining of both proteins was performed as in Fig. 2***F*** (*left* part). The biotinylation assay was performed as in Fig. 2***G*** (*right* part). In (***C***) and (***D***), tubulin and IgM were used as loading controls for input and biotinylation, respectively. The representative results of three independent experiments are presented.

Figure 4. Multiple sequence alignment of TMDs II and V among hZnT transporters. The sequences of TMDs II and V of hZnT transporters were aligned. The sequence order is according to their sequence similarity (41). The conserved His and Asp residues postulated as the Zn-binding site in TMDs II and V are highlighted in orange and blue. Residue N43 in TMD II of hZnT10 is highlighted in green. C52 and L242 residues of hZnT10 that were investigated in Fig. 9 are shown in red. The indicated TMDs of hZnT5 correspond to TMDs XI and XIV.

Figure 5. Asn residue in TMD II of hZnT10 is essential for Mn transport activity. ***A***, expression of hZnT10$_{(hZnT1Cter)}$ did not alter Mn resistance in *SPCA1*$^{-/-/-}$ cells. ***B***, expression of hZnT10$_{(hZnT1Cter)}$ did not confer Zn resistance in *ZnT1*$^{-/-}$*MT*$^{-/-}$*ZnT4*$^{-/-}$ cells. ***C***, expression of hZnT10$_{(hZnT1Loop)}$ did not alter Mn resistance in *SPCA1*$^{-/-/-}$ cells. ***D***, expression of hZnT10$_{(hZnT1Loop)}$ did not confer Zn resistance in *ZnT1*$^{-/-}$*MT*$^{-/-}$*ZnT4*$^{-/-}$ cells. ***E***, expression of hZnT10$_{(N43H)}$ significantly decreased Mn resistance in *SPCA1*$^{-/-/-}$ cells. ***F***, expression of hZnT10$_{(N43H)}$ did not confer Zn resistance in *ZnT1*$^{-/-}$*MT*$^{-/-}$*ZnT4*$^{-/-}$ cells. In (***A***), (***C***), and (***E***), or in (***B***), (***D***), and (***F***), cells were grown as in Fig. 3***A*** and ***B***, and the numbers of living cells were evaluated by the Alamar Blue assay. In (***A***)–(***F***), the Alamar Blue assay was performed at least three times. Confirmation of stable expression of WT and mutants of hZnT10 in *SPCA1*$^{-/-/-}$ cells or *ZnT1*$^{-/-}$*MT*$^{-/-}$*ZnT4*$^{-/-}$ cells by immunoblotting (*lower* panels). Tubulin is shown as a loading control. ***G***, the cell surface localization of hZnT10 mutants in *SPCA1*$^{-/-/-}$ cells was evaluated by the surface biotinylation assay. ***H***, the cell surface localization of hZnT10 mutants in *ZnT1*$^{-/-}$*MT*$^{-/-}$*ZnT4*$^{-/-}$ cells was evaluated by the surface biotinylation assay. In (***G***) and (***H***), the biotinylation assay was performed as in Fig. 2***G***. The representative results of three independent experiments are presented.

Figure 6. Substitution of Asn residue for His residue in TMD II confers the activity to transport Mn with hZnT1. ***A***, expression of hZnT1$_{(hZnT10Cter)}$ did not confer Mn resistance in *SPCA1*$^{-/-/-}$ cells. ***B***, expression of hZnT1$_{(hZnT10Cter)}$ did not alter Zn resistance in *ZnT1*$^{-/-}$*MT*$^{-/-}$*ZnT4*$^{-/-}$ cells. ***C***, expression of hZnT1$_{(hZnT10Loop)}$ did not confer Mn resistance in *SPCA1*$^{-/-/-}$ cells. ***D***, expression of hZnT1$_{(hZnT10Loop)}$ did not alter Zn resistance in *ZnT1*$^{-/-}$*MT*$^{-/-}$*ZnT4*$^{-/-}$ cells. ***E***, expression of hZnT1$_{(H43N)}$ did confer Mn resistance in *SPCA1*$^{-/-/-}$ cells. ***F***, expression of hZnT1$_{(H43N)}$ lost the ability to confer Zn resistance in *ZnT1*$^{-/-}$*MT*$^{-/-}$*ZnT4*$^{-/-}$ cells. In (***A***), (***C***), and (***E***), or in (***B***), (***D***), and (***F***), cells were grown as in Fig. 3***A*** and ***B***, and the numbers of living cells were evaluated by the Alamar Blue assay. In (***A***)–(***F***), the Alamar Blue assay was performed at least three times. Confirmation of stable WT and mutants of hZnT1 expression in *SPCA1*$^{-/-/-}$ cells or *ZnT1*$^{-/-}$*MT*$^{-/-}$*ZnT4*$^{-/-}$ cells by immunoblotting (*lower* panels).

Tubulin and calnexin are shown as the loading controls. ***G***, the cell surface localization of hZnT1 mutants in *SPCA1*$^{-/-}$ cells was evaluated by the surface biotinylation assay. ***H***, the cell surface localization of hZnT1 mutants in *ZnT1*$^{-/-}$*MT*$^{-/-}$*ZnT4*$^{-/-}$ cells was evaluated by the surface biotinylation assay. In (***G***) and (***H***), hZnT1$_{(hZnT10Cter)}$ was detected by an anti-hZnT10 antibody, whereas WT ZnT1 and other hZnT1 mutants were detected by an anti-hZnT1 antibody. The biotinylation assay was performed as in Fig. 2***G***. The representative results of three independent experiments are displayed.

Figure 7. Domain swapping and substitution analysis between hZnT10 and hZnT2. ***A***, expression of hZnT2$_{(H106N)}$ failed to confer Mn resistance in *SPCA1*$^{-/-}$ cells. ***B***, expression of hZnT2$_{(H106N)}$ lost the ability to confer Zn resistance in *ZnT1*$^{-/-}$*MT*$^{-/-}$*ZnT4*$^{-/-}$ cells. ***C***, expression of hZnT10$_{(hZnT2Cter)}$ lost the ability to confer Mn resistance in *SPCA1*$^{-/-}$ cells. ***D***, expression of hZnT10$_{(hZnT2Cter)}$ did not confer Zn resistance in *ZnT1*$^{-/-}$*MT*$^{-/-}$*ZnT4*$^{-/-}$ cells. ***E***, expression of hZnT2$_{(hZnT10Cter)}$ did not confer Mn resistance in *SPCA1*$^{-/-}$ cells. ***F***, expression of hZnT2$_{(hZnT10Cter)}$ lost the ability to confer Zn resistance in *ZnT1*$^{-/-}$*MT*$^{-/-}$*ZnT4*$^{-/-}$ cells. In (***A***), (***C***), and (***E***), or in (***B***), (***D***), and (***F***), cells were grown as presented in Fig. 3***A*** and ***B***, and the numbers of living cells were evaluated by the Alamar Blue assay. In (***A***)–(***F***), the Alamar Blue assay was performed at least three times. Confirmation of stable expression of WT and mutants of hZnT2 and hZnT10 in *SPCA1*$^{-/-}$ cells or *ZnT1*$^{-/-}$*MT*$^{-/-}$*ZnT4*$^{-/-}$ cells by immunoblotting (*lower* panels). Tubulin is shown as the loading control.

Figure 8. Domain swapping and substitution of specific sequences failed to be compatible between hZnT10 and hZnT2. ***A***, expression of hZnT10$_{(N43H\text{-}hZnT2Loop\text{-}hZnT2Cter)}$ lost the ability to confer Mn resistance in *SPCA1*$^{-/-}$ cells. ***B***, expression of hZnT10$_{(N43H\text{-}hZnT2Loop\text{-}hZnT2Cter)}$ did not confer Zn resistance in *ZnT1*$^{-/-}$*MT*$^{-/-}$*ZnT4*$^{-/-}$ cells. ***C***, expression of hZnT2$_{(H106N\text{-}hZnT10Loop\text{-}hZnT10Cter)}$ did not confer Mn resistance in *SPCA1*$^{-/-}$ cells. ***D***, expression of hZnT2$_{(H106N\text{-}hZnT10Loop\text{-}hZnT10Cter)}$ lost the ability to Zn resistance in *ZnT1*$^{-/-}$*MT*$^{-/-}$*ZnT4*$^{-/-}$ cells. In (***A***) and (***C***), or in (***B***) and (***D***), cells were grown as presented in Fig. 3***A*** and ***B***, and the numbers of living cells were evaluated by the Alamar Blue assay. In (***A***)–(***F***), Alamar Blue assay was performed at least three times. Confirmation of stable expression of WT and mutants of hZnT2 and hZnT10 in *SPCA1*$^{-/-}$cells or *ZnT1*$^{-/-}$*MT*$^{-/-}$*ZnT4*$^{-/-}$ cells by immunoblotting (*lower* panels). Tubulin is shown as the loading control.

Figure 9. Residues C52 and L242 in the TMDs II and IV of hZnT10 are involved in the control of metal substrate specificity in hZnT10. ***A***, expression of hZnT10$_{(N43H,\ C52V)}$ did not confer Zn resistance in *ZnT1*$^{-/-}$*MT*$^{-/-}$*ZnT4*$^{-/-}$ cells. ***B***, expression of hZnT10$_{(N43H,\ L242F)}$ did not confer Zn resistance in *ZnT1*$^{-/-}$*MT*$^{-/-}$*ZnT4*$^{-/-}$ cells. ***C***, expression of hZnT10$_{(N43H,\ C52V,\ L242F)}$ and hZnT10$_{(N43H,\ C52V,\ L242F\text{-}hZnT1Cter)}$ partially restored the ability to confer Zn resistance in *ZnT1*$^{-/-}$*MT*$^{-/-}$*ZnT4*$^{-/-}$ cells. ***D***, expression of hZnT10$_{(N43H\text{-}hZnT1Cter)}$ did not confer Zn resistance in *ZnT1*$^{-/-}$*MT*$^{-/-}$*ZnT4*$^{-/-}$ cells. ***E***, expression of hZnT10$_{(C52V,\ L242F)}$ did not confer Zn resistance in *ZnT1*$^{-/-}$*MT*$^{-/-}$*ZnT4*$^{-/-}$ cells. ***F***, expression of hZnT10$_{(C52V,\ L242F)}$ did not impair Mn resistance in *SPCA1*$^{-/-}$ cells. In (***A***)–(***E***), or in (***F***), cells were grown as presented in Fig. 3***A*** and ***B***, and the numbers of living cells were evaluated by the Alamar Blue assay. The Alamar Blue assay was performed at least three times in (***A***), (***B***), and (***D***)–(***F***), and four times in (***C***). Confirmation of stable expression of hZnT10 mutants in *SPCA1*$^{-/-}$ cells or *ZnT1*$^{-/-}$*MT*$^{-/-}$*ZnT4*$^{-/-}$ cells by immunoblotting (*lower* panels). Tubulin is shown as the loading control.

Table 1. Conferment of Mn and Zn resistance by hZnT10 or hZnT1 and their domain swapped/substituted mutants in *SPCA1*$^{-/-/-}$ and *ZnT1*$^{-/-}$*MT*$^{-/-}$*ZnT4*$^{-/-}$ cells

Expressed gene	Mn resistance in *SPCA1*$^{-/-/-}$ cells	Zn resistance in *ZnT1*$^{-/-}$*MT*$^{-/-}$*ZnT4*$^{-/-}$ cells
hZnT10	+++	–*
hZnT1	–	+++
$hZnT10_{(N43H)}$	–*	–
$hZnT1_{(H43N)}$	+++	–
$hZnT10_{(hZnT1Cter)}$	+++	–
$hZnT1_{(hZnT10Cter)}$	–	++
$hZnT10_{(hZnT1Loop)}$	+++	–
$hZnT1_{(hZnT10Loop)}$	–	+++

Relative values presented are evaluations of the results shown in Figures 3, 5, and 6 as follows. +++: >75% viability compared with that of WT in *SPCA1*$^{-/-/-}$ cells at 40 μM $MnSO_4$ or that of WT in *ZnT1*$^{-/-}$*MT*$^{-/-}$*ZnT4*$^{-/-}$ cells at 60 μM $ZnSO_4$; ++, +: less growth (25–75%, or ≤ 25% relative to the viability of each WT); –: no growth; * a small fraction of the cells appeared morphologically normal by visual observation.

Table 2. Conferment of Mn and Zn resistance by hZnT10 or hZnT2 and their domain swapped/substituted mutants in *SPCA1*$^{-/-/-}$ and *ZnT1*$^{-/-}$*MT*$^{-/-}$*ZnT4*$^{-/-}$ cells

Expressed gene	Mn resistance in *SPCA1*$^{-/-/-}$ cells	Zn resistance in *ZnT1*$^{-/-}$*MT*$^{-/-}$*ZnT4*$^{-/-}$ cells
hZnT10	+++	–*
hZnT2	–	+++
$hZnT10_{(N43H)}$	–	–
$hZnT2_{(H106N)}$	–	–
$hZnT10_{(hZnT2Cter)}$	–	–
$hZnT2_{(hZnT10Cter)}$	–	–*
$hZnT10_{(N43H\text{-}hZnT2Loop\text{-}hZnT2Cter)}$	–	–
$hZnT2_{(H106N\text{-}hZnT10Loop\text{-}hZnT10Cter)}$	–	–

Relative values presented are evaluations of the results shown in Figures 7 and 8, as described in Table 1.

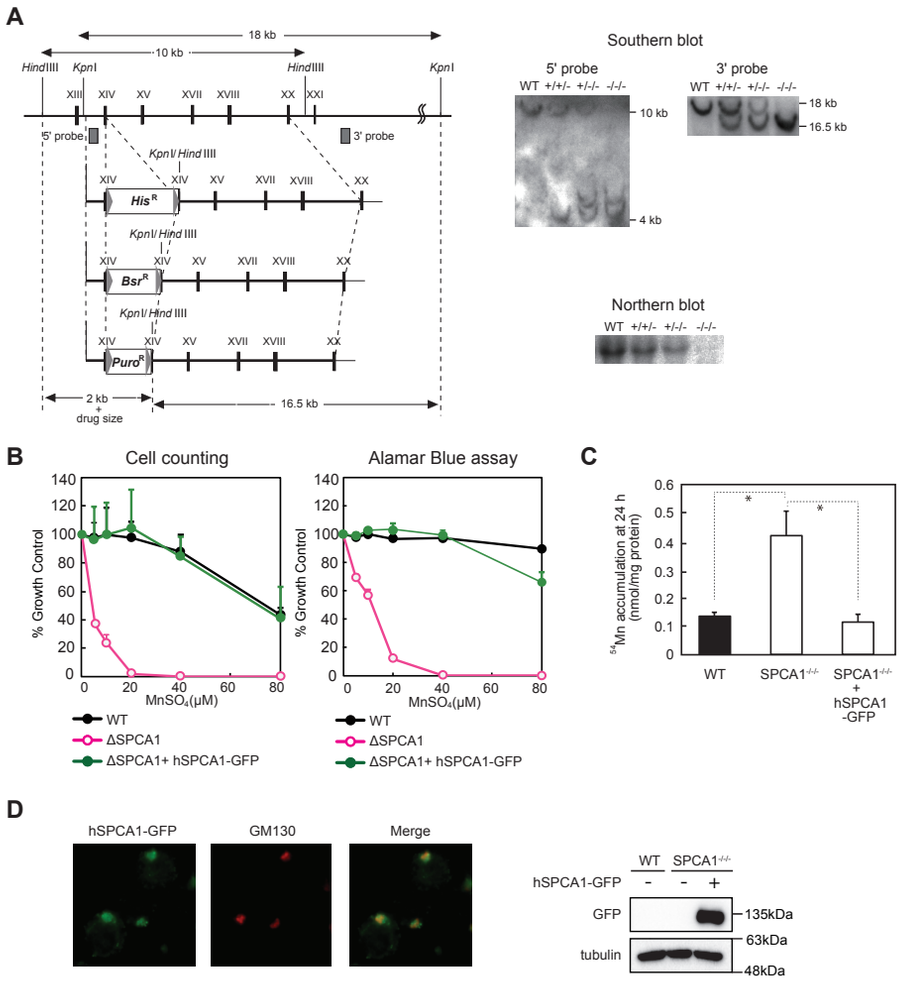

Figure 1

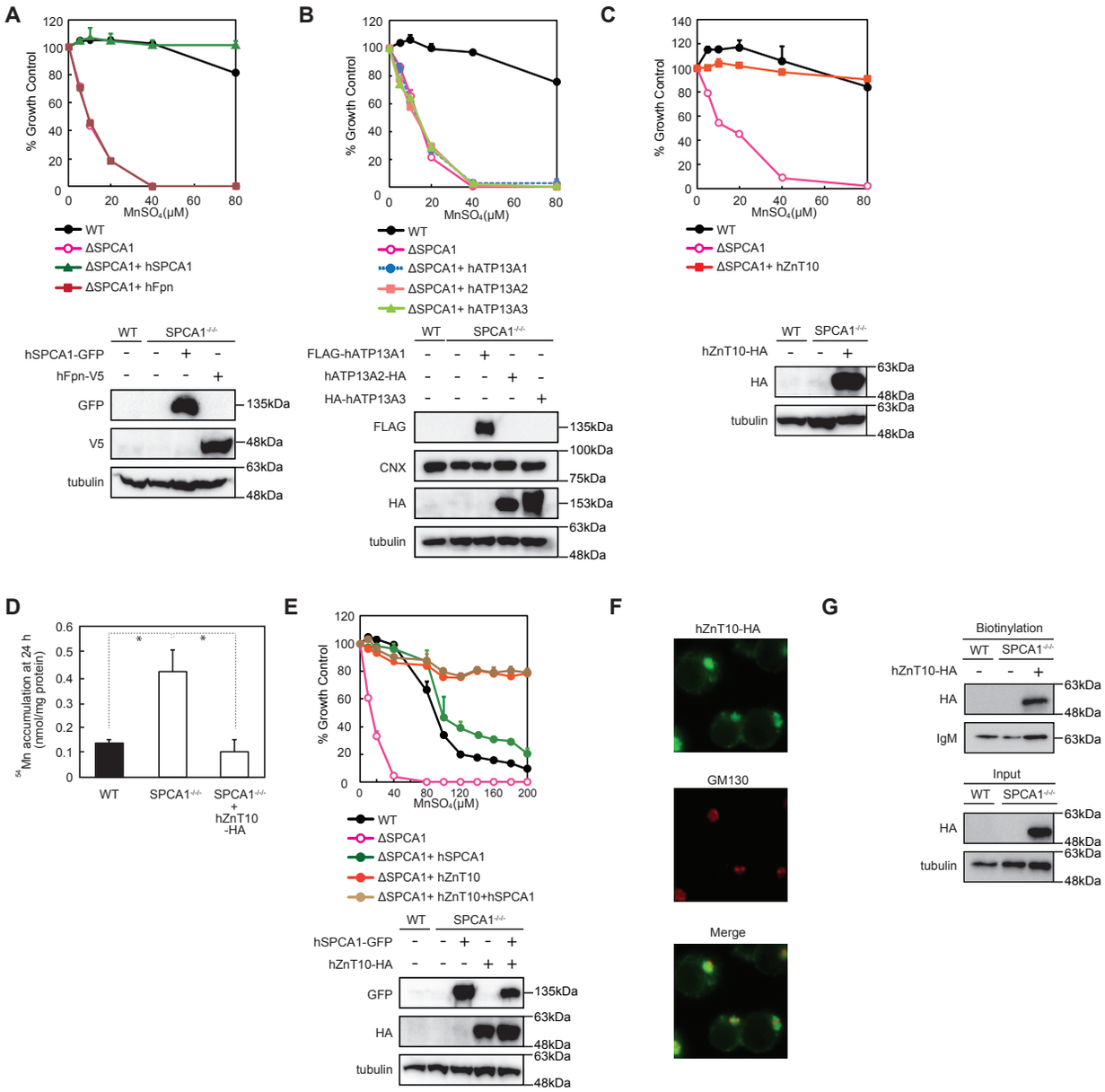

Figure 2

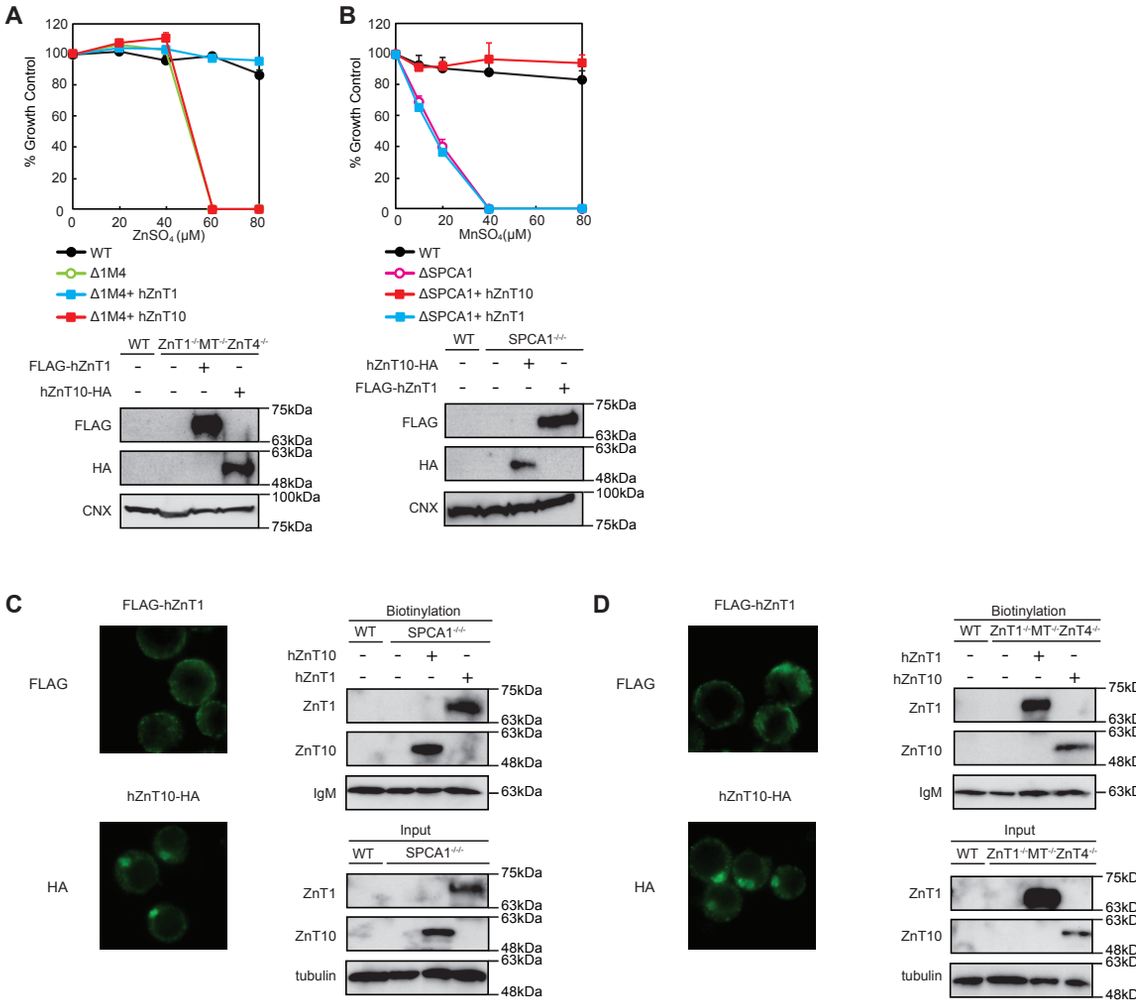

Figure 3

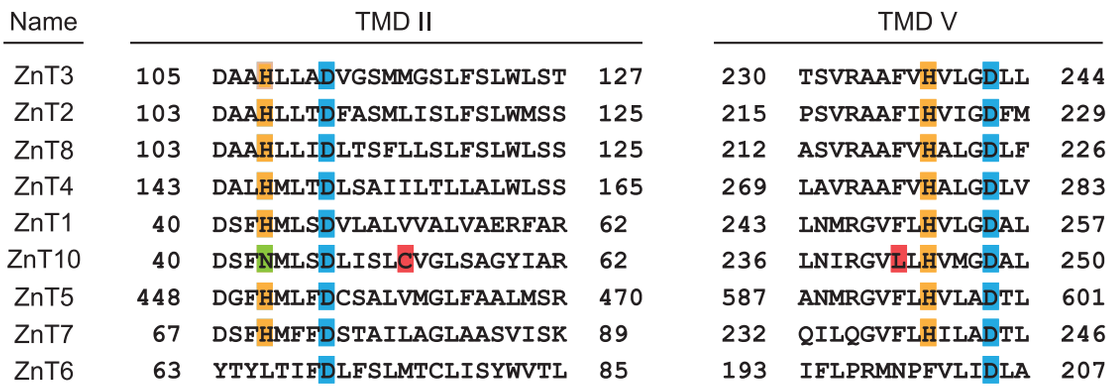

Figure 4

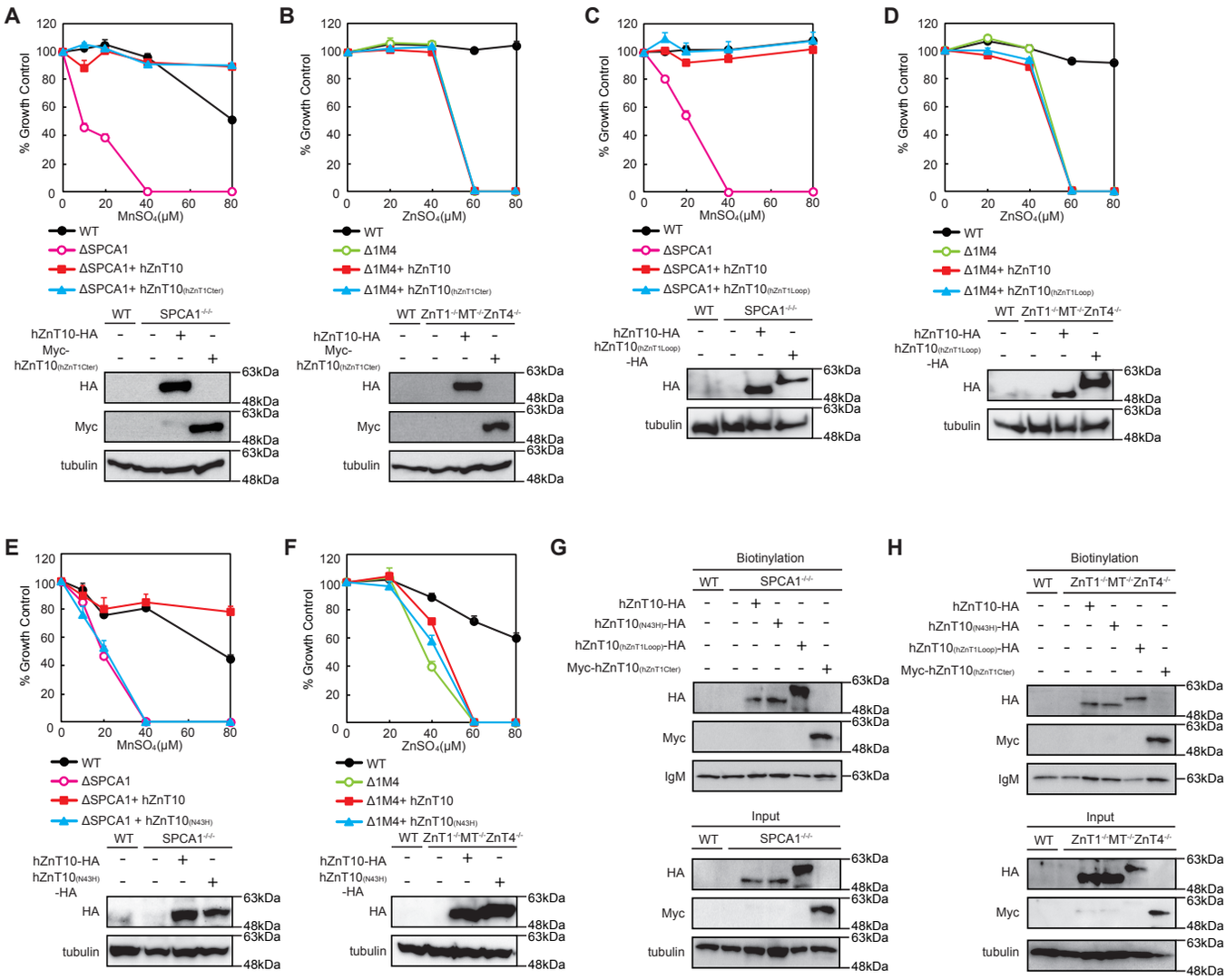

Figure 5

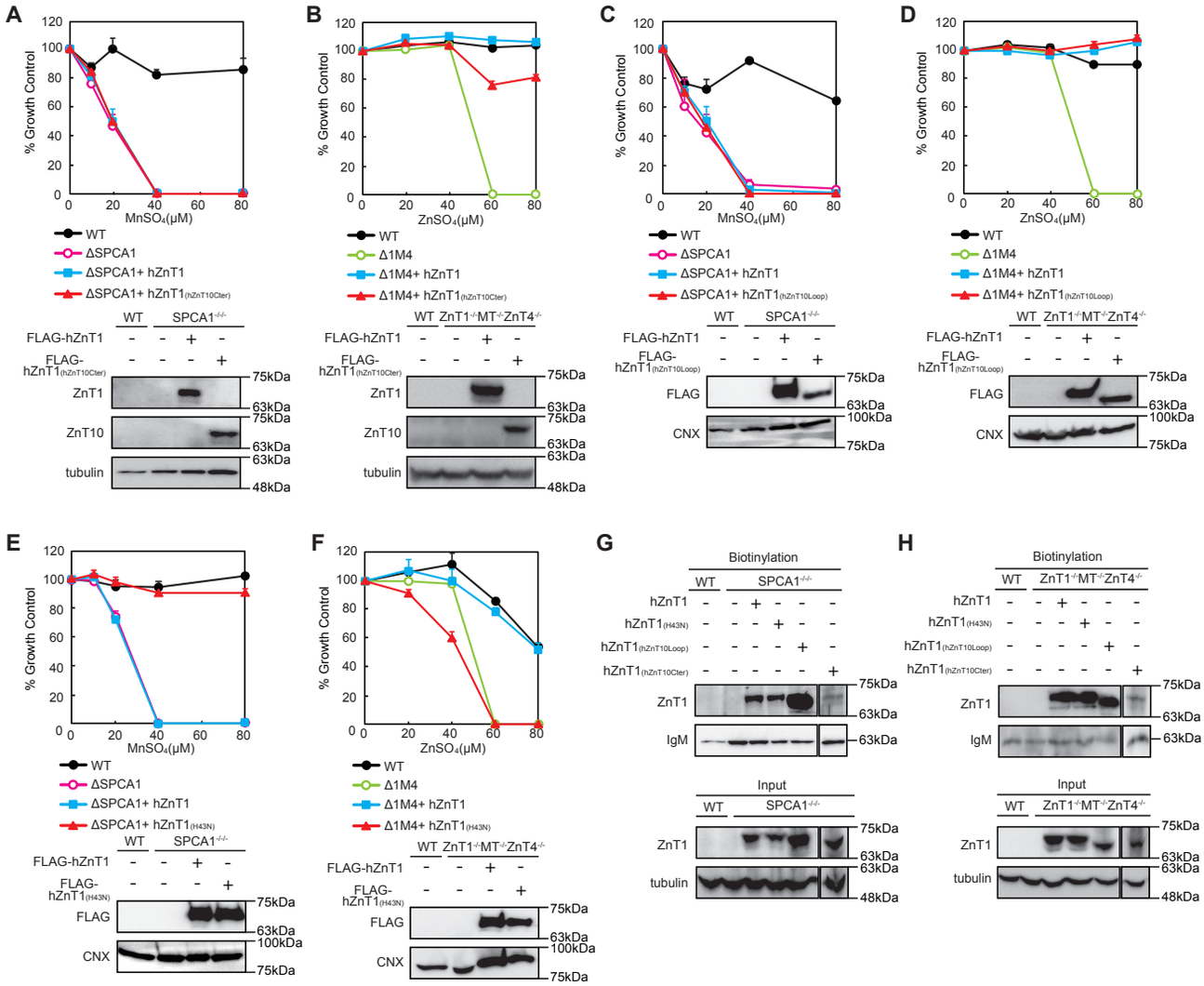

Figure 6

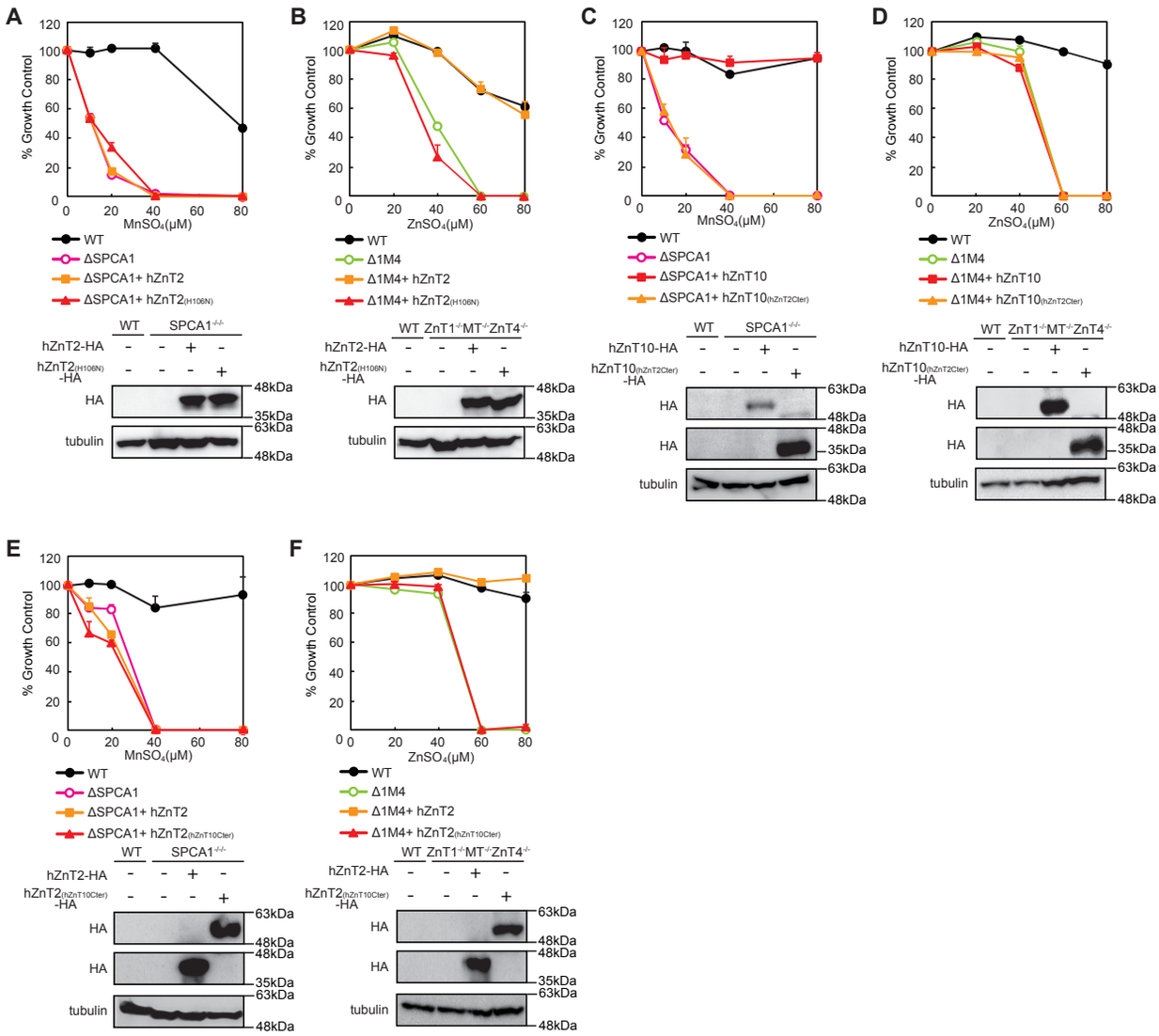

Figure 7

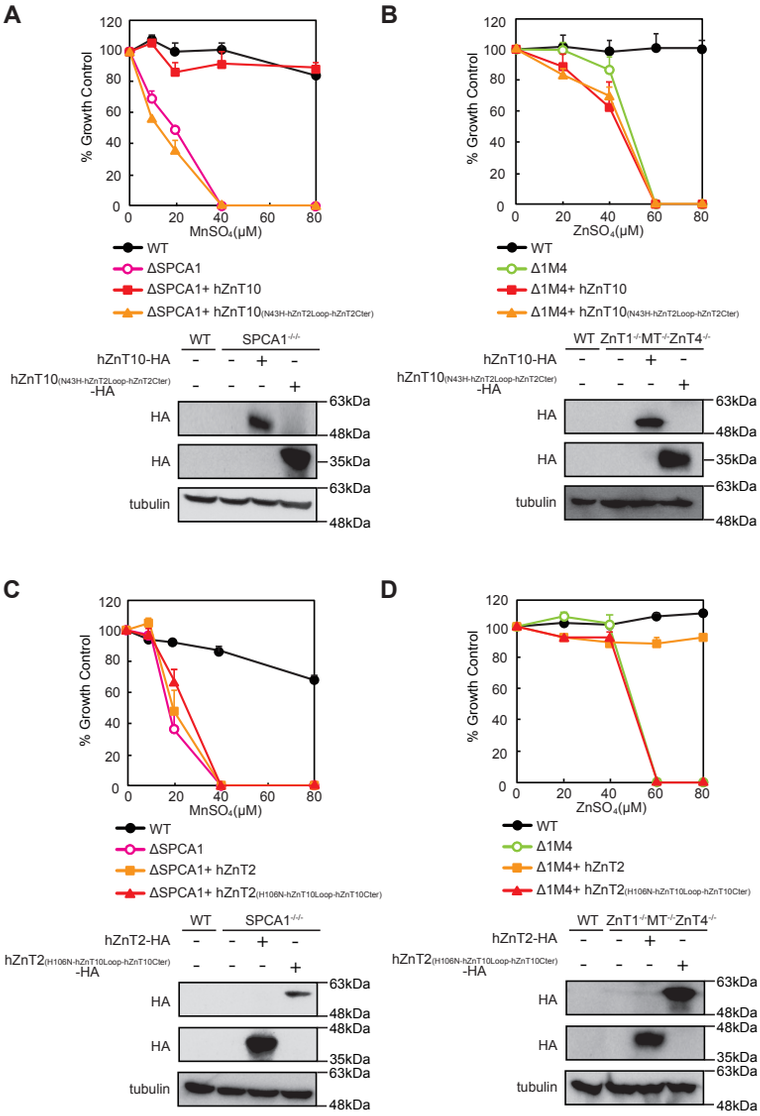

Figure 8

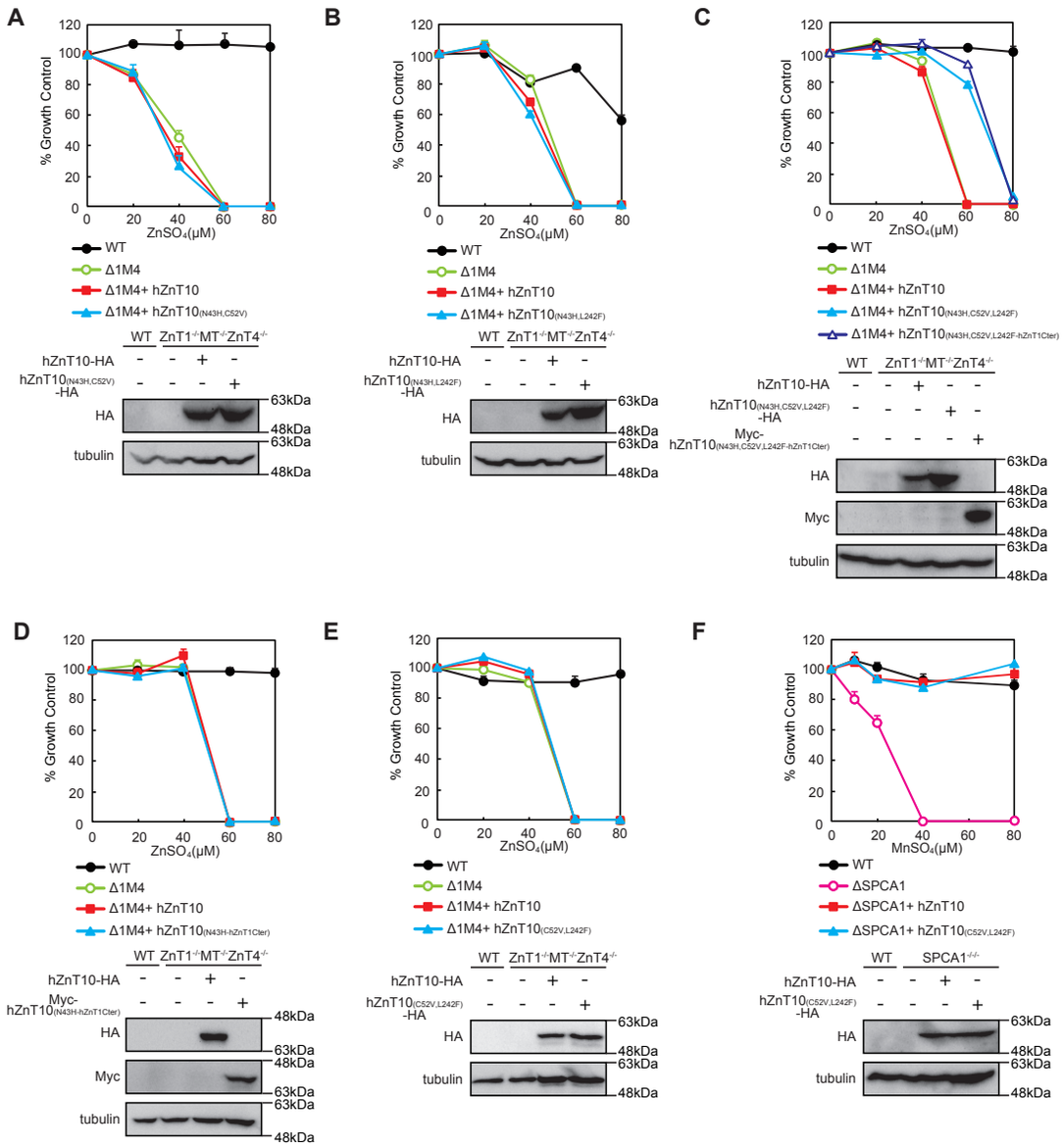

Figure 9

Direct Comparison of Manganese Detoxification/Efflux Proteins and Molecular Characterization of ZnT10 as a Manganese Transporter

Yukina Nishito, Natsuko Tsuji, Hitomi Fujishiro, Taka-aki Takeda, Tomohiro Yamazaki, Fumie Teranishi, Fumiko Okazaki, Ayu Matsunaga, Karin Tuschl, Rajini Rao, Satoshi Kono, Hiroaki Miyajima, Hiroshi Narita, Seiichiro Himeno and Taiho Kambe

J. Biol. Chem. published online May 10, 2016
